A systematic study of multi-octave spectral broadening in a hollow core capillary

Eine systematische Studie eines in einer Hohlkernkapillare erzeugten oktav-weiten Superkontinuums

Michael Heynck

München 2021

A systematic study of multi-octave spectral broadening in a hollow core capillary

Michael Heynck

Masterarbeit
an der Fakultät für Physik
der Ludwig-Maximilians-Universität
München

vorgelegt von
Michael Heynck
aus Landshut

München, den 13.09.2021

Betreuer: Prof. Dr. Ferenc Krausz
Projektleiter: Dr. Matthew Weidman

Contents

Abstract

A useful tool in the world of ultra fast physics is an optical waveform synthesizer. This device takes a several octave spanning spectrum and splits it up into individual channels. Each of them allows the compression of the narrower spectral region. A subsequent combination delivers ultra short sub-cycle laser pulses that are needed in the field of ultra fast physics. Within the framework of this thesis, the generation of this necessarily octave spanning spectrum happens by sending a beam centred at a wavelength of 2 µm into a gas filled hollow core capillary for spectral broadening. The generated supercontinuum covers a range from 300 nm to 3000 nm. The aim of this thesis is to characterise it with emphasize on how the gas, the pressure and the pulse energy influence the spectral broadening. Of particular interest is the origin of a strong spectral peak in the ultra violet, which is found out to be a dispersive wave. Accompanying numerical simulations shall support the understanding of the measured spectra. And since the next generation synthesizer, that is currently being built, will also use a 2 µm beam for spectral broadening, the outcome of this thesis can be utilized to determine the spectral range of the new generated supercontinuum.

List of Abbreviations

BBO	beta barium borate
CEP	carrier envelope phase
CPA	chirped pulse amplification
EOI	electro optic imaging
EOS	electro optic samlping
FWM	four wave mixing
GD	group delay
GDD	group delay dispersion
GVD	group velocity dispersion
GNLSE	generalized nonlinear Schrödinger equation
HCF	hollow core fibre
NIR	near infrared
NLSE	nonlinear Schrödinger equation
PPLN	periodically poled lithium niobate
RDW	resonant dispersive wave
SPM	self phase modulation
UV	ultra violet
VIS	visible
WL	white light
XPM	cross-phase modulation
Yb:YAG	ytterbium-doped yttrium aluminium garnet
ZDW	zero dispersion wavelength

List of Figures

List of Tables

Introduction

Ultra fast physics is a field where phenomena, that happen on the time scale of the oscillations of a light field, are discovered and explained. This, for example, includes the observation of electron motions in atoms and molecules as well as the deeper understanding of nonlinear interactions of light fields with different kinds of media. All of this is only possible if some sort of measuring signal exists that is short enough in time and has sufficient intensity. And it indeed does, in form of ultrashort light pulses, where the electric field is described by a few cycles of the oscillations of the light field. These pulses can even get so short that they only consist of less than a period of the oscillating filed, thus building a sub cycle transient.

The generation of ultrashort sub-cycle pulses is a challenging task. The laser system used for the measurements of this thesis though can produce these pulses. This starts with an optical parametric amplifier that delivers a beam centred at 2 µm. The spectral bandwidth is however not large enough to enable sub-cycle pulses. To broaden the spectrum to the extent to make single transients possible, this beam is sent to a hollow core capillary waveguide, where the high laser intensity causes spectral broadening and thus supercontinuum generation.

To finally deliver sub-cycle transients, the pulses need to be temporally compressed since they are dispersed from the broadening process. This is a demanding task, as the spectrum reaches now 300 nm to 3000 nm, so covering a range of three octaves. The used tool to achieve this is called an optical waveform synthesizer. With this device, the whole spectrum is split up into three channels. Each channel is compressed on its own, and if needed, can also be altered by controlled applied dispersion. Therefore, the resulting pulse shape can be a sub-cycle transient if all three compressed channels are combined or whatever is possible given the rich variety of combinations.

The laser system currently used is operating at 3 kHz and the 2 µm beam that is broadened has 1 mJ pulse energy. The next generation laser system also delivers a beam at the same wavelength, but at a higher repetition rate of 50 kHz. However, this beam should have a pulse energy of 80 µJ. Since the new laser system is going to be equipped with an optical waveform synthesizer to make use of its widespread applications, it needs to be determined if the necessary broadening with less pulse energy can be achieved in order to have the same or

better bandwidth than the currently used synthesizer. The aim of this thesis is to characterize the supercontinuum that is generated if a 2 µm beam with 80 µJ pulse energy is sent into a gas filled hollow core fibre. Of particular interest is the comprehensive description of a spectral peak in the ultra violet, as it did not happen yet. Both this detailed description and the whole analysis of the super continuum is supported by numerical simulations.

The outline of this thesis is as follows: Chapter 1 starts with giving the theoretical background to understand the processes that lead to the generated supercontinuum including the peak in the ultra violet, which is called dispersive wave. It starts showing a mathematical description of ultra short pulses and continuous by presenting an important equation, the generalized non linear Schrödinger equation. This equation will be numerically solved to revise the experimental measurements done and also to figure out if the used program is capable of simulating the correct spectra. The chapter continues by explaining the main processes that lead to the generation of a supercontinuum. This includes the mechanism of self phase modulation that is generally the reason for broadening if a high intense pulse is sent into a gas filled hollow core fibre. But it also includes the special case that is encountered here, where the input pulse is a soliton that generates a resonant dispersive wave in the ultra violet.

Chapter 2 gives an overview of the system currently used. It describes how the 2 µm beam is generated that is utilized to produce a supercontinuum that is send to the current synthesizer. For this thesis, the beam is sent to another system, build up just to characterize the generated spectrum. This setup is a gas filled hollow core fibre, where both the gas pressure and the input pulse energy can be adjusted. The output beam is captured by two spectrometers, covering a range from 200 nm to 2500 nm.

Chapter 3 focuses on analysing the captured spectra. Two different kinds of measurements were performed, during one the input pulse energy was changed and in the other one the pressure. The evaluation happened by finding out how the generation of the supercontinuum, including the dispersive wave, is dependent on the gas, the pressure and the pulse energy. This made it possible to understand the shape of the broadband spectrum entering the current synthesizer, as well as to make a prediction of the spectrum that is used for the next generation synthesizer that is part of the new system with 80 µJ pulse energy.

Chapter 4 discusses the viability of the utilized program to do the numerical simulations of super continuum generation. For that, selected measured spectra are compared to numerical solutions. Moreover, the simulated behaviour of spectral broadening inside the fibre is examined and compared to what is expected from a theoretical point of view.

The thesis ends with chapter 5. Here, the findings of the last two preceding chapters are shortly summarized. Going on from that, the spectrum of the next generation synthesizer and the possibility of generating a dispersive wave on purpose is discussed.

Chapter 1

Theoretical Background

The purpose of this chapter is to provide the necessary theoretical background to understand the most important physical principles that are covered by this thesis. It starts with section 1.1 giving a mathematical description of ultrashort pulses. To get a more detailed description [1] may be consulted. The propagation inside a medium of these pulses will be discussed in section 1.2. In the end, an equation shall be given that describes what happens if a pulse is sent into a gas filled hollow core fibre. This equation is solved numerically in chapter 4 to see if the result matches the measured spectra in chapter 3. To see a more detailed derivation, it should be referred to [2] and [3]. This equation describes different physical processes, which are addressed in the following. Section 1.3 covers the most important nonlinear processes that arise from high intensity laser pulses. To get a more in depth understanding of the derivation of these effects, [2], [3] and [4] should be read. To further better understand the origin of the spectral peak in the ultra violet, something that will be observed in chapter 3, section 1.4 discusses what happens if linear dispersion and nonlinear effects as in section 1.3 are interacting and thus making solitons and dispersive waves possible. A more detailed description for that can be found in [2], [3], [4], [5], [6], [7] and [8].

1.1 Description of Ultrashort Pulses

The field of an ultrashort pulse is completely described through a real valued electromagnetic wave. Both the electric field and the magnetic field of such a wave are not completely independent and can thus be derived from each other by the Maxwells's equations. In the following, a description of the electric field only is given. Without simplifying too much, the field is only described by its temporal component, so no spatial or polarization dependence. The electric field $E(t)$ in the time domain can be equivalently described in the frequency domain. The complex field in the frequency domain $\tilde{E}(\omega)$ is obtained by using the Fourier transform:

$$\tilde{E}(\omega) = \int_{-\infty}^{+\infty} E(t)e^{-i\omega t}dt = |\tilde{E}(\omega)|e^{i\phi(\omega)}, \tag{1.1}$$

where $|\tilde{E}(\omega)|$ is the spectral amplitude and $\phi(\omega)$ is the frequency dependent spectral phase. With the inverse Fourier transform, the real electric field $E(t)$ can be calculated form the given complex spectrum $\tilde{E}(\omega)$:

$$E(t) = \frac{1}{2\pi}\int_{-\infty}^{+\infty} \tilde{E}(\omega)e^{i\omega t}d\omega. \tag{1.2}$$

To describe the propagation of a wave, it is useful to define a complex electric field in time, which can be achieved in two ways:

$$\tilde{E}^{+}(t) = \frac{1}{2\pi}\int_{0}^{\infty} \tilde{E}(\omega)e^{i\omega t}d\omega = \frac{1}{2\pi}\int_{-\infty}^{+\infty} \tilde{E}^{+}(\omega)e^{i\omega t}d\omega. \tag{1.3}$$

One way is to perform the Fourier transform of the complex spectrum only for positive frequencies, the other way is to perform a full Fourier transform, but define $\tilde{E}^{+}(\omega)$ in a way that it is zero for all negative frequencies and equal to $\tilde{E}(\omega)$ for all positive frequencies. In the same way $\tilde{E}^{-}(t)$ can be obtained by a full Fourier transform of $\tilde{E}^{-}(\omega)$. In this case $\tilde{E}^{-}(\omega)$ is defined in a way that it is equal to $\tilde{E}(\omega)$ for all negative frequencies and zero for all positive frequencies. This gives

$$\tilde{E}(\omega) = \tilde{E}^{+}(\omega) + \tilde{E}^{-}(\omega). \tag{1.4}$$

With that it is possible to rewrite the electric field as

$$E(t) = \tilde{E}^{+}(t) + \tilde{E}^{-}(t). \tag{1.5}$$

With $\tilde{E}^{+}(t)$ being a complex function, it is possible to express it as an amplitude function $A(t)$ multiplied by term containing the phase information $\Phi(t)$:

$$\tilde{E}^{+}(t) = A(t)e^{i\Phi(t)} = A(t)e^{i(\phi_0+\phi(t)+\omega_0 t)}. \tag{1.6}$$

Here, the phase consists of three terms, namely ϕ_0 being the carrier envelope phase (CEP), $\phi(t)$ the time dependent phase and ω_0 the carrier frequency. The carrier frequency describes the oscillations of the electric field under the envelope. The relative phase between the envelope and the oscillating field is described by the CEP. For ultrashort pulses, the CEP is an important value since the maximum field amplitude depends on it, see figure 1.1.

The time dependent phase $\phi(t)$ is important for the instantaneous frequency, which is defined as:

$$\omega(t) = \omega_0 + \frac{d}{dt}\phi(t). \tag{1.7}$$

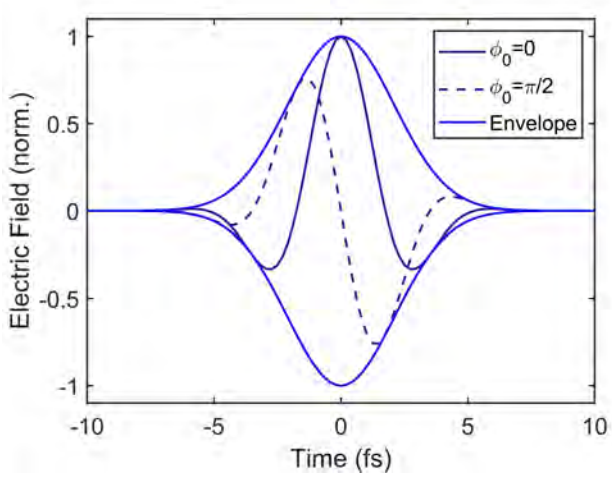

Figure 1.1: Envelope and electric field of an ultra short pulse with two different values for the CEP.

As a consequence of this, the frequency of the carrier signal can vary in time as the pulse propagates. A specific change of $\omega(t)$, by making certain assumptions for $\phi(t)$, will be discussed in section 1.3.1 and 1.4.1.

Sometimes it is useful to describe the phase in the frequency domain. For that, one can write $\tilde{E}^+(\omega)$ in a similar way to equation 1.1 as:

$$\tilde{E}^+(\omega) = |\tilde{E}^+(\omega)|e^{i\phi(\omega)}, \tag{1.8}$$

where $\phi(\omega)$ is the frequency dependent phase. Like the time dependent phase, it can be expressed through multiple terms, as it happens by describing it by a Taylor series around ω_0:

$$\phi(\omega) = \phi(\omega_0)+\frac{d}{d\omega}\phi(\omega)\Big|_{\omega=\omega_0}(\omega-\omega_0)+\frac{1}{2}\frac{d^2}{d\omega^2}\phi(\omega)\Big|_{\omega=\omega_0}(\omega-\omega_0)^2+\frac{1}{6}\frac{d^3}{d\omega^3}\phi(\omega)\Big|_{\omega=\omega_0}(\omega-\omega_0)^3+... \tag{1.9}$$

The first term describes the phase propagation of the electric filed, so the carrier below the envelope. The second term, also called group delay (GD), describes the propagation of the whole pulse, so the envelope. The third term is called group delay dispersion (GDD). This and the following higher order terms describe the frequency dependent propagation of each individual wavelength component of the electric field. If they are unequal zero, the pulse shape gets altered. In section 1.4.1, the influence of the GDD on a pulse will be discussed in more detail.

1.2 Propagation of Ultrashort Pulses

So far, the electric field was just a function of time. For the propagation inside of a medium, it is necessary to take a more universally valid approach. For that, the electric field can have a polarization and is dependent of space coordinates. In the case of cartesian coordinates, the electric field becomes $\boldsymbol{E}(x, y, z, t)$. To describe the propagation of such a field, the Maxwell equations are needed. For a medium that is source free, without currents ($\rho = 0$, $\boldsymbol{J} = \vec{0}$) and non magnetic, the Maxwell equations will take the following form:

$$\nabla \cdot \boldsymbol{D} = 0, \tag{1.10}$$

$$\nabla \cdot \boldsymbol{B} = 0, \tag{1.11}$$

$$\nabla \times \boldsymbol{E} = -\frac{\partial \boldsymbol{B}}{\partial t}, \tag{1.12}$$

$$\nabla \times \boldsymbol{H} = \frac{\partial \boldsymbol{D}}{\partial t}, \tag{1.13}$$

with the electric and magnetic flux density

$$\boldsymbol{D} = \epsilon_0 \boldsymbol{E} + \boldsymbol{P}, \qquad \boldsymbol{B} = \mu_0 \boldsymbol{H}, \tag{1.14}$$

where ϵ_0 is the permittivity and μ_0 is the permeability. With both of them the speed of light in vacuum can be calculated by:

$$c = \frac{1}{\sqrt{\epsilon_0 \mu_0}}. \tag{1.15}$$

From the Maxwell equations and the flux densities, a nonlinear wave equation for the electric field can be derived and takes the following form:

$$\left(\nabla^2 - \frac{1}{c^2}\frac{\partial^2}{\partial t^2}\right)\boldsymbol{E}(x, y, z, t) = \frac{1}{\epsilon_0 c^2}\frac{\partial^2}{\partial t^2}\boldsymbol{P}(x, y, z, t) \tag{1.16}$$

where $\nabla = (\frac{\partial}{\partial x}, \frac{\partial}{\partial y}, \frac{\partial}{\partial z})$ is the nabla operator. The polarization $\boldsymbol{P}$ on the right hand side describes the materials response to an electric field of a light pulse. As a consequence of this response, the electric field will be changed during propagation through a medium. For very high intensity laser pulses, the polarization can be split up in two terms

$$\boldsymbol{P} = \boldsymbol{P}_L + \boldsymbol{P}_{NL}. \tag{1.17}$$

The linear response of the material is represented through $\boldsymbol{P}_L$. Effects like dispersion, diffraction and linear attenuation are describes by this term. Nonlinear effects, that occur only for high intensities, are represented through $\boldsymbol{P}_{NL}$. Some

of these effects are discussed in more detail in section 1.3. It is further possible to express the polarization in a series expansion, which gives for the case of an instantaneous response:

$$\boldsymbol{P} = \epsilon_0(\chi^{(1)}\boldsymbol{E} + \chi^{(2)}\boldsymbol{E}^2 + \chi^{(3)}\boldsymbol{E}^3 + ...), \tag{1.18}$$

where the first order term is the linear polarization and all higher order terms are the nonlinear polarization. The $\chi^{(n)}$ are the n-th order susceptibilities.

By neglecting all nonlinearities and applying a Fourier transform to 1.16, one can get:

$$\left(\nabla^2 + n^2(\omega)\frac{\omega^2}{c^2}\right)\boldsymbol{E}(x, y, z, \omega) = 0, \tag{1.19}$$

which has the form of a Helmholtz equation, with $n(\omega)$ being the refractive index following the relationship $n^2(\omega) = 1 + \chi^{(1)}(\omega)$. A plane wave approach will give the following solution for propagation along the z-axis:

$$E(z, t) = E_0 e^{i(\omega_0 t - k_0 z)} \tag{1.20}$$

with the wave number $k_0 = n^2(\omega_0)\omega_0^2/c^2$ and ω_0 the center angular frequency.

A more general approach is to include nonlinearities and using the frequency dependent wave number $\beta(\omega)$, which leads to:

$$[\nabla^2 + \beta^2(\omega)]\boldsymbol{E}(x, y, z, \omega) = -\frac{\omega^2}{\epsilon_0 c^2}\boldsymbol{P}_{NL}(x, y, z, \omega). \tag{1.21}$$

To describe the propagation of a pulse inside a gas filled fibre, it first has to be noted that all even order terms in the series expansion in 1.18 vanish since the medium has inversion symmetry. To find a simpler expression, some assumptions have to be made. These are: (i) the nonlinearities are weak compared to the linear contribution to the polarization, (ii) the pulse is propagating along the z direction and is linearly polarized, with the polarizations being conserved, (iii) the dispersion is weak and iv) the slowly varying envelope approximation can be applied, which requires $\Delta\omega/\omega_0 << 1$, with $\Delta\omega$ the pulse bandwidth. Under these conditions, the electric field can be expressed as:

$$E(x, y, z, \omega) = F(x, y)A(z, \omega)e^{i\beta(\omega)z}. \tag{1.22}$$

$F(x, y)$ is the transverse mode distribution and can be expressed as the distribution of a HE_{nm} mode. $A(z, \omega)$ is the slowly varying mode amplitude.

With this expression for the electric field, starting from equation 1.21, a new wave equation can be derived. This takes the form:

$$\frac{\partial A}{\partial z} + \beta_1\frac{\partial A}{\partial t} + i\frac{\beta_2}{2}\frac{\partial^2 A}{\partial t^2} + \frac{\alpha}{2}A = i\gamma(\omega_0)|A|^2 A, \tag{1.23}$$

with $\beta_k = \frac{d^k\beta}{d\omega^k}|_{\omega=\omega_0}$ the Taylor expansion coefficients, α the attenuation constant and γ the nonlinear coefficient. Both α and γ depend on properties of the medium the pulse propagates through. An expression for them shall be given at the end of this section. The proportionality of the nonlinear contribution on the right hand side to $|A|^2A$ originates form the third nonlinear part in expression 1.18, which is the first nonlinear part in this case given the preconditions made that all even orders vanish.

This equation describes the propagation of a pulse through a dispersive, nonlinear medium. The dispersion goes up to the second order, the nonlinearity is limited to $\chi^{(3)}$ processes like self phase modulation (SPM), which is described in section 1.3. With an appropriate coordinate transform it is possible to further simplify this equation. By neglecting the attenuation α and setting $\tau = t - z/v_g$, with v_g the group velocity, the time frame changes to a copropagating system that travels alongside the pulse. The result is the nonlinear Schrödinger equation (NLSE) 1.44, which will be discussed in section 1.4.2. To treat the propagation of laser pulses more properly, it is useful to use the generalised non linear Schrödinger equation (GNLSE), which can take the following form:

$$\frac{\partial A}{\partial z} = -\frac{\alpha}{2}A - \left(\sum_{n=2}^{\infty}\beta_n\frac{i^{n-1}}{n!}\frac{\partial^n}{\partial t^n}\right)A + i\gamma\left(1+\frac{1}{\omega_0}\frac{\partial}{\partial t}\right)|A|^2A. \tag{1.24}$$

Compared to equation 1.23 there are two changes. At first, the dispersion is not limited to the second order, meaning that the full dispersion of the medium can be taken into consideration. This is especially of importance for ultrashort pulses since they are also ultra broadband. Second, an additional nonlinear term appeared. This term describes the effect of self steepening, which will be described in section 1.3. This equation can also contain more terms describing additional effects, like the Raman response. But since only noble gases are used for this thesis, this term is omitted. This equation will be solved numerically in chapter 4 to simulate the supercontinuum generated and discussed in chapter 3.

Now the expressions for α, γ and $\beta(\omega)$ for the propagation of a gas filled hollow core fibre shall be given. The attenuation constant has the form [9]:

$$\alpha = 2\left(\frac{u_{nm}}{2\pi}\right)^2\frac{\lambda_0^2}{2a^3}\frac{\nu^2+1}{\sqrt{\nu^2-1}}, \tag{1.25}$$

where $\nu = n_{fibre}/n_{gas}$ is the ratio of the refractive index of the fibre cladding and the gas. λ_0 is the center wavelength of the laser and a the core radius of the fibre. u_{nm} is the m^{th} root of the Bessel function $J_{n-1}(u_{nm})$. For the fundamental mode it is: $u_{11} = 2.405$. The nonlinear parameter is defined as [9]:

$$\gamma = \frac{n_2\omega_0}{cA_{eff}}, \tag{1.26}$$

with ω_0 the central angular frequency of the pulse, c the speed of light and $A_{eff} \approx 0.48\pi a^2$ the effective mode area. n_2 is the nonlinear refractive index and is given by [7]:

$$n_2 = n_2^0 \frac{p}{p_0} \frac{T_0}{T}, \tag{1.27}$$

with p and T the pressure in bar and the temperature in Kelvin of the gas, $p_0 = 1\,\text{bar}$ and $T_0 = 273\,\text{K}$. The values for n_2^0 can be taken from table 1.1. Since the nonlinear refractive index is also wavelength dependent, the following

Gas	n_2^0 ($10^{-24}\text{m}^2/\text{W}$)	I_p(eV)
He	0.41	24.59
Ne	0.74	21.56
Ar	10.40	15.76
Kr	29.14	14.00
Xe	93.50	12.13

Table 1.1: Values of n_2^0 at 800 nm and the ionization potential for different noble gases [10], [11].

formula can be used to calculate n_2^0 for different wavelengths [10]:

$$n_2^0(\omega) = \frac{\nu\omega' - \omega_p}{\nu\omega - \omega_p} n_2^0(\omega'), \tag{1.28}$$

with $\nu = \frac{3}{2}$ and ω_p the angular frequency of the connected ionization potential. The dispersion of a gas filled hollow core fibre is given by [7]:

$$\beta(\omega) = \frac{\omega}{c}\sqrt{n_{gas}^2 - \frac{u_{nm}^2 c^2}{a^2\omega^2}}, \tag{1.29}$$

where the refractive index of the gas can be calculated with the following Sellmeier equation [12]:

$$n^2 - 1 = \frac{p}{p_0}\frac{T_0}{T}\left[\frac{B_1\lambda^2}{\lambda^2 - C_1} + \frac{B_2\lambda^2}{\lambda^2 - C_2}\right], \tag{1.30}$$

with λ the wavelength in µm, p the pressure in bar, T the temperature in Kelvin, $p_0 = 1\,\text{bar}$, $T_0 = 273\,\text{K}$ and B_1, B_2, C_1, C_2 constants given in table 1.2

1.3 Nonlinear effects

It was already mentioned that a laser field with high intensity causes the material to respond in a nonlinear way. To account for that, the polarization was extended to also include higher order terms $\chi^{(n)}\boldsymbol{E}^n$. These terms take the nonlinear response into consideration, since they are now of the order $\boldsymbol{E}^n$ and n can

Gas	$B_1 \cdot 10^8$	$C_1 \cdot 10^6$	$B_2 \cdot 10^8$	$C_2 \cdot 10^3$
He	4977.77	28.54	1856.94	7.760
Ne	9154.48	656.97	4018.63	5.728
Ar	20332.29	206.12	34458.31	8.066
Kr	26102.88	2.01	56946.82	10.043
Xe	103701.61	12.75	31228.61	0.561

Table 1.2: Constants of different noble gases for equation 1.30 [12]

be larger than 1. Generally, the $\chi^{(n)}$ are complex tensors of rank (n+1). The series expansion done in equation 1.18 requires an immediate response of the material. By making this assumption and by observing that noble gases have inversion symmetry, so that all even order terms vanish, the first and strongest nonlinear term contributing to the nonliner polarization is:

$$P_{NL} = \epsilon_0 \chi^{(3)} E^3. \tag{1.31}$$

This equation shows that the resulting polarization will have oscillations build up by E^3. The frequency of the oscillating polarization is determined by adding and/or subtracting the frequency of three waves that are part of the electric field that goes through the medium. This process is called Four Wave Mixing (FWM), since three input waves mix and create a new fourth wave. Besides of energy conversation, which demands that the energy contained in the new created wave is equal to the total energy of the original three waves, there is also a so called phase matching condition. This requires that the wavevector of the created wave is equal to the sum of the mixing waves. If a monochromatic wave of the form $E = E_0(e^{i\omega t} + e^{-i\omega t})$ is taken as the input for equation 1.31, the resulting polarization will have two different frequency components. One will oscillate at 3ω and one at ω. The first describes third harmonic generation, since the new wave has three times the frequency. For this process, one has to take account for phase matching. The latter describes the so called optical Kerr effect. Here, the resulting frequency is equal to the incoming one and thus phase matching is automatically fulfilled. For this case, equation 1.31 can take the following form:

$$P_{NL} = 3\epsilon\chi^{(3)}|E|^2 E. \tag{1.32}$$

Since the Intensity can be written as $I = 2n_0\epsilon_0 c|E|^2$, it can be seen that the nonlinear polarization is proportional to the intensity of the incoming light pulse. This results in an intensity dependent refractive index of the form

$$n = n_0 + n_2 I, \tag{1.33}$$

with n_2 defined as in 1.27 and n_0 the refractive index of a light beam without a high intensity, so $n_0 = \sqrt{1 + \chi^{(1)}}$. This intensity dependence is also called optical Kerr effect. There are several phenomena that follow from this behaviour of n, which will be discussed in the following sections.

1.3.1 Self Phase Modulation (SPM)

In order to understand the effect of SPM, it is useful to consider a plane wave propagating along the z-axis: $E(z,t) = E_0 e^{i(\omega t - kz)}$, with the wavevector $k = \frac{\omega}{c} n$. If equation 1.33 is taken as the refractive index n for this plane wave ansatz one gets:

$$k = \frac{\omega}{c} n = \frac{\omega}{c}(n_0 + n_2 I(t)). \tag{1.34}$$

This results in the electric field

$$E(z,t) = E_0 e^{i(\omega t - \frac{\omega}{c}(n_0 + n_2 I(t))z)}. \tag{1.35}$$

If the light propagates the distance D, the phase shift due to the intensity dependent refractive index is

$$\phi(t) = -\frac{\omega}{c} n_2 I(t) D. \tag{1.36}$$

The change of the spectrum can be derived by putting this into equation 1.7, which leads to an instantaneous frequency of

$$\omega(t) = \omega_0 - n_2 \frac{\omega}{c} \frac{dI(t)}{dt} D. \tag{1.37}$$

From this it can be seen that the instantaneous frequency of the pulses carrier changes as the time dependent intensity varies. If a pulse with Gaussian shape is assumed, the leading part of the pulse would get red shifted, since $dI/dt > 0$ and as a result the frequency $\omega(t)$ gets smaller. For the trailing edge it is the other way around. There, the frequency gets blue shifted, as $dI/dt < 0$. This is shown in figure 1.2.

This change of the frequency leads to spectral broadening of the laser pulse, since after SPM the pulse has more frequency components than before. The spectrum of a Gaussian pulse can be seen in figure 1.3 for different propagation distances. It is symmetric, so the shape of the blue shifted spectrum is the same as for the red shifted part.

1.3.2 Self-Steepening

Another process that happens because of the intensity dependent refractive index is self steepening. To understand this process, it is helpful to calculate the group delay as it is defined in equation 1.9 as the first derivative of the phase. By using equation 1.34 again, one obtains the phase $\phi = kD = \frac{\omega_0}{c}(n_0 + n_2 I(t))D$ with D being the propagation distance one more time. This results in the group delay:

$$\frac{\partial \phi}{\partial \omega} = D \frac{\partial k}{\partial \omega} = D \frac{\omega_0}{c} \frac{\partial (n_2 I(t))}{\partial \omega} = \frac{D}{v_{gr}}, \tag{1.38}$$

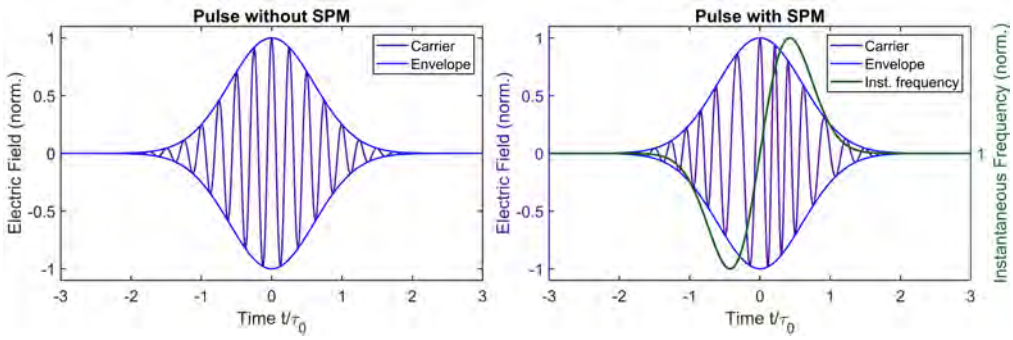

Figure 1.2: The change of the carrier of a Gaussian pulse due to SPM. On the left, the original pulse can be seen. On the right, the carriers instantaneous frequency changes according to the green curve, with a red shift on the left (leading edge) and a blue shift on the right (trailing edge). At the center, the instantaneous frequency is equal to ω_0.

where the derivative of the wavevector k is defined as $\frac{\partial k}{\partial \omega} = 1/v_{gr}$, with v_{gr} the the velocity of a pulse inside a medium, also called group velocity. Following from this, the velocity of a pulse is inversely proportional to its own intensity. This correlates with the refractive index being proportional to the intensity of the pulse. This effect alters the pulse shape as the high intensity peak will be slowed down, since it will experience a higher refractive index and thus a lower group velocity. The edges on the other hand are not intense enough to change the refractive index and will propagate with the original, faster group velocity. Assuming again a Gaussian pulse, the following will happen: The peak, due to the high intensity, will be slowed down. As the velocity of the edges will remain unchanged, the peak starts to move towards the trailing edge, as it can be seen in figure 1.4. With increasing propagation distance, the trailing edge becomes steeper and steeper, until a point it reached when it is vertical and the pulse will break up. This event is then called optical shock.

Not only the pulse shape in time is affected by self steepening, also the spectrum gets altered. Due to SPM, which happens in parallel to self steppening, the spectrum is broadened symmetrically, as it was shown in figure 1.3. However, due to the contribution of self steepening, the spectrum becomes asymmetrically. Self steepening now extends the spectral range in the higher frequency region, by also lowering the spectral amplituden as it is illustrated in figure 1.5. This is explained through the form of the trailing edge. In order to have a steep edge in the time domain, much more high frequency components are needed than low frequency components. And since the power contained the this blue part is the same as in the red part, the spectral amplitude decreases.

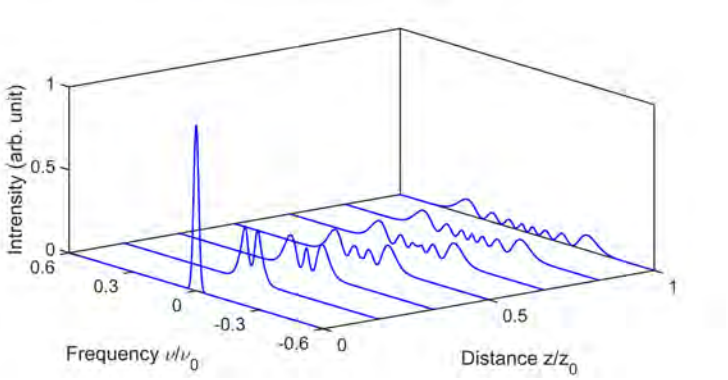

Figure 1.3: Spectrum of a Gaussian pulse as it propagates through a medium and gets broadened due to SPM. The spectrum is symmetric to the center at ω_0.

1.3.3 Self Focusing

So far, the effect of the intensity dependent refractive index only changed the pulse spectrum and envelope due to the temporal intensity profile. But also the spatial distribution can change due to this effect. If the beam has a higher intensity at the center, then this part will see an increased total refractive index compared to the rest of the beams spatial profile. As a result, the material will behave like a lens and the beam will start to focus. This can go on and on until the diffraction of the beam, whose strength increases as the beam is focusing, will compensate for the focusing effect. The state when the diffraction and the focusing cancel each other out is then called self-trapping, since the beam diameter will stay unchanged during propagation. The critical parameter for this to happen is the so called critical power for self focusing, which is given by [3]:

$$P_{cr} = \frac{\pi(0.61)^2\lambda_0^2}{8n_0n_2}. \tag{1.39}$$

If the power of the beam reaches this value, then self-trapping can occur. If the power is much larger, than the beam will break up in many transverse distributed beams, with each of them having the critical power.

1.4 Soliton dynamics

1.4.1 Dispersion

Now it shall be discussed a bit more in detail what happens to a pulse if it propagates through a dispersive medium. For that, the frequency dependent refractive index and therefore the frequency dependent wavevector are needed.

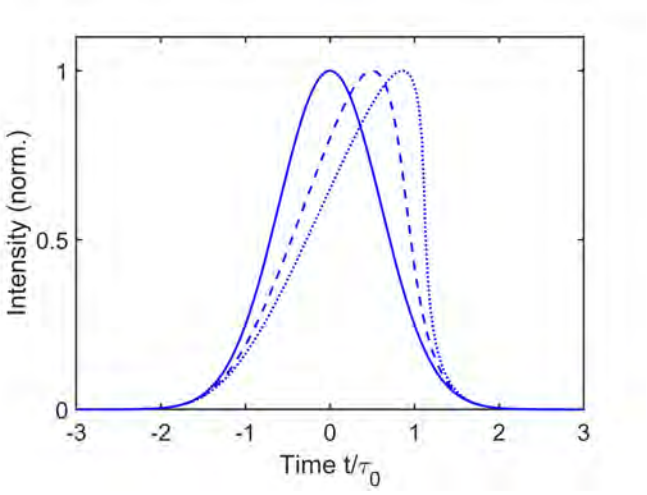

Figure 1.4: Self steepening of a Gaussian pulse. The original pulse (solid line) gets steeper with propagation distance (dashed line). Close to the optical shock the trailing edge is almost vertical (dotted line).

With that, the phase for each frequency component of the pulse can be evaluated. It was shown in equation 1.9 that the phase can be described in in a Taylor series. By using the relationship between the phase and the wavevector $\phi = \beta D = \frac{\omega}{c} n D$, with the the propagated distance D, one can also do a Taylor expansion of $\beta(\omega)$, which gives:

$$\beta(\omega) = \beta_0 + \beta_1(\omega - \omega_0) + \frac{1}{2}\beta_2(\omega - \omega_0)^2 + \frac{1}{6}\beta_3(\omega - \omega_0)^3 + ... \tag{1.40}$$

with the beta coefficients:

$$\beta_n = \frac{d^n}{d\omega^n}\beta(\omega)\bigg|_{\omega=\omega_0}. \tag{1.41}$$

Each of these beta coefficients have a different impact on the pulse. The first two terms were already mentioned in section 1.1. The zero-order term describes the phase velocity. This value gives information about how fast the phase information of a pulse travels. The first order term describes the group velocity, which is the speed of the pulse itself. What was not discussed yet are the second and higher order terms. These are of particular interest since they can alter the shape of the pulse. The second-order term is called group velocity dispersion (GVD), and it describes how the group velocity changes with frequency. This is a result of the dispersion relation, so the fact that the refractive index is frequency dependent. If the value for the GVD is unequal zero, it means that waves with different frequencies travel at different speeds. Due to that, the pulse end up being chirped. Depending of the sign of β_2, either the red frequencies are

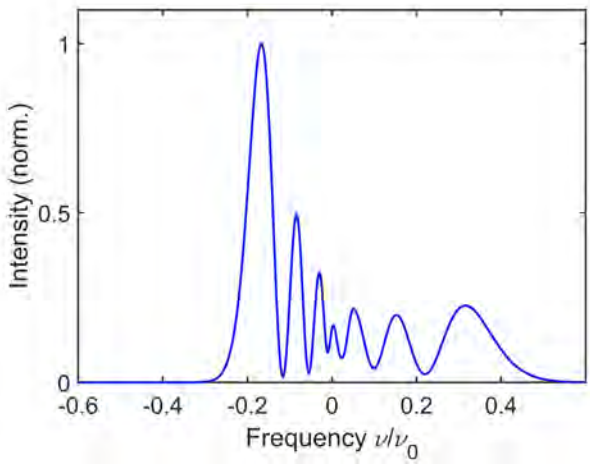

Figure 1.5: The antisymmetric spectrum of a Gaussian pulse after SPM and self steepening. The blue part of a symmetric spectrum from SPM gets stretched to support the steep trailing edge in the time domain.

faster or the blue ones. It is convention to speak of normal dispersion if the red components are leading and the blue ones are trailing. This leads to a positive chirp. In this case $\beta_2 > 0$. In the other case, it is called anomalous dispersion, here $\beta_2 < 0$ and the blue frequencies are in the leading edge of the pulse and the red are trailing, which leads to a negative chirp. This can be seen in figure 1.6. Both normal and anomalous dispersion will stretch the pulse, since each wave is

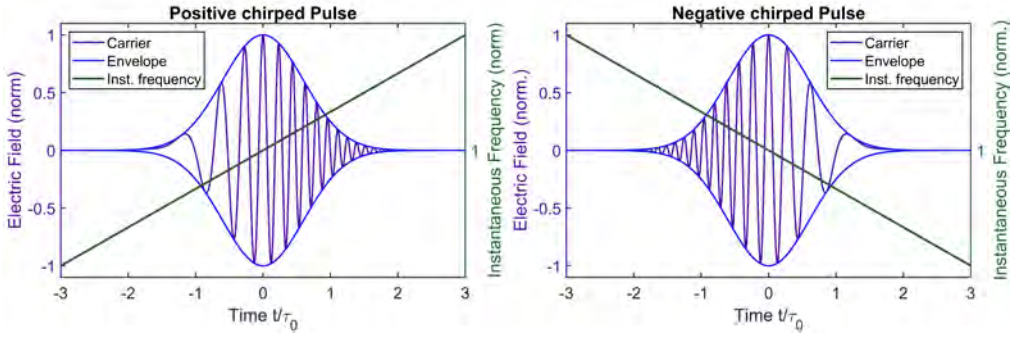

Figure 1.6: On the left $\beta_2 > 0$, so the red frequency are leading and the pulse gets a positive chirp. On the right $\beta_2 < 0$, so the red frequencies are trailing, which gives the pulse a negative chirp.

travelling with its own speed. For gas filled hollow core fibres, as they are used in this thesis, there will be a wavelength region where the dispersion is normal and a region where it is anomalous. In-between there is a point where the GVD

will reach a value of zero. This is called the zero-dispersion-wavelength (ZDW), and describes which wavelength will propagate without dispersion.

This is dispersion due to the linear part of the polarization. But it was also shown in section 1.3.1 that the nonlinear contribution of SPM can change the pulse phase in a comparable way, namely that the pulse gets a positive chirp. In difference to normal dispersion, here the high intensity causes a phase shift. In the case of linear dispersion, only the materials properties causes different frequencies experiencing different phase changes. The interesting case of a high intensity beam propagating though a material where the pulse lies in the anomalous liner dispersion regime and also experiences SPM will be discussed in the next subsection. If a pulse propagates through a medium, it is useful to estimate the change to it coming from linear dispersion and nonlinear effects. For that, two length scales exist, which describe roughly after which propagation distance the pulses phase gets altered. These are the dispersion length

$$L_D = \frac{\tau_0^2}{|\beta_2|}, \tag{1.42}$$

and the nonlinear length

$$L_{NL} = \frac{1}{\gamma P_0}, \tag{1.43}$$

with τ_0 describing the duration and P_0 the peak power of the input pulse. If the propagation length reaches one of these lengths, the connected effect will affect the pulse. If the two length scales are comparable with the propagation length, both will simultaneously change the pulse. This will be the case in the next subsection.

1.4.2 Solitons

It was mentioned in section 1.2 that one can arrive at the nonlinear Schrödinger equation if only linear dispersion and SPM are affecting a propagating pulse. The equation has the form:

$$\frac{\partial A}{\partial z} = -i\frac{\beta_2}{2}\frac{\partial^2 A}{\partial T^2} + i\gamma|A|^2 A. \tag{1.44}$$

There are several special solutions to this equation that all describe the same type of pulses: optical solitions. These solitons have the unique property that the pulses shape either remains unchanged during propagation or it oscillates, but always reaches the original pulse shape after a specific distance. The fundamental soliton never changes the shape. All higher order solitions will periodically change the shape, both in time and frequency domain. But after one oscillation they will come to the starting shape. This behaviour is shown in figure 1.7. The soliton order can be expressed as a function of the dispersion length L_D and the

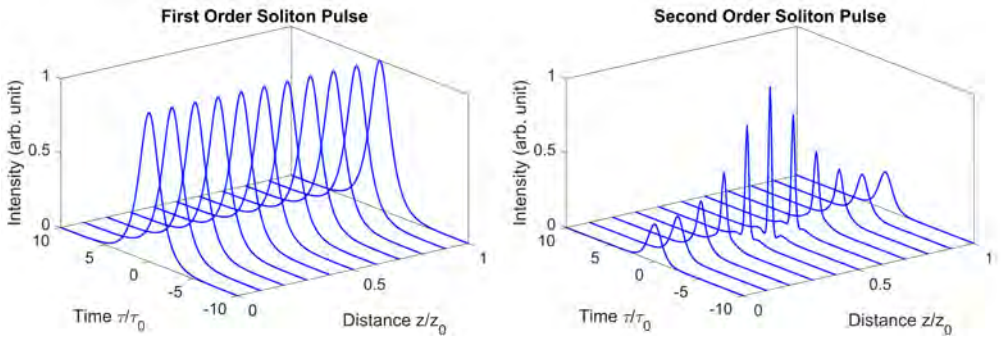

Figure 1.7: On the left, the propagation of a first order soliton is shown, where the shape never changes. On the right, a full oscillation of a second order soliton is shown.

nonlinear length L_{NL} from section 1.4.1:

$$N = \sqrt{\frac{L_D}{L_{NL}}}. \tag{1.45}$$

The behaviour of a soliton can be understood by taking a look again at how SPM and linear dispersion change the pulse. It was mentioned that SPM causes a positive chirp of a propagating pulse. If there is in addition normal dispersion the pulse would be even more chirped, so a soliton would not be possible under these conditions. But if the linear dispersion is anomalous, the negative chirp can compensate the positive chirp coming from SPM. Under these conditions a soliton can exist. For the fundamental soliton, SPM and dispersion compensate each other exactly. For higher order solitions, there is an interplay between them, which results in oscillations. What all the higher order solitons have in common, is that at first the spectum is broadened due to SPM. Then the negative dispersion compensates for the positive chirp induced by SPM and the pulse will be compressed. Since the spectrum is more broadband now, the pulse will be shorter than in the beginning. With only SPM and dispersion up to β_2, the pulse would reach a point of maximum spectral width and so a point of maximal temporal compression and then continues with the oscillating process until the original pulse shape and spectrum is reached. But in a system like a gas filled hollow core fibre, there are additional processes like self steepening and also higher order terms for the dispersion, starting from β_3, are not zero. This has a strong impact on the behaviour of soliton propagation. For a solition of order $N > 1$, in the beginning of the propagation there will be broadening through SPM and self compression due to the negative dispersion. But as the pulse spectrum gets broader and broader and the pulse gets shorter and shorter in time, the pulse will break up at some point. During the break up the higher order

soliton will merge into several lower order solitons. This process is therefore also called soliton fission and the associated length scale is given by:

$$L_{fiss} = \frac{L_D}{N} = \sqrt{L_D L_{NL}} \tag{1.46}$$

While broadening happens and the fission has not occurred yet, the spectrum can extend till the normal dispersive region of the hollow core fibre. This region covers all wavelengths that are smaller than the zero dispersion wavelength, and thereby also smaller than the pulses spectrum in the beginning is. Due to the higher order dispersion coefficients, the phase velocity for a small spectral region in the normal region can overlap with the phase velocity of the soliton pulse. In other words, the phasematching conditions are given in this case. This leads to a resonant transfer of energy from the soliton in this so called dispersive wave, hence the name resonant dispersive wave (RDW). The name originates form the fact that the wave is propagating in the normal dispersion region of the fibre. The necessary phasematching condition for this process is:

$$\beta(\omega) - \beta_{sol}(\omega) = \beta(\omega) - \beta(\omega_0) - \beta_1(\omega_0)(\omega - \omega_0) - \Phi = 0. \tag{1.47}$$

with $\beta(\omega)$ describing the linear mode propagation constant, so the wavenumber as in section 1.4.1 and ω_0 the center angular frequency of the soliton. Φ is a phase terms that describes the additional phase a soliton has. By solving the NLSE one can show that this term is equal to [5]

$$\Phi = \frac{\gamma P_0}{2}, \tag{1.48}$$

with P_0 the peak power of the soliton. If the temporal compression of the soliton is taken into account, the peak power can be replaced by the peak power of the compressed pulse $P_c = P_0 F_c$ [6]. With the compression factor given by $F_c \sim 4.6N$, which is obtained from simulations, the resulting phase term becomes:

$$\Phi = 2.3N\gamma P_0. \tag{1.49}$$

By introducing a shock-term ω/ω_0 [13], one can get the following expression for the phase term:

$$\Phi = \frac{\omega}{\omega_0}\gamma P_0. \tag{1.50}$$

If self compression is assumed once again one can replace the term for the peak power with $4.5NP_0$ [8], it results in:

$$\Phi = 4.5N\frac{\omega}{\omega_0}\gamma P_0. \tag{1.51}$$

With the phasematching condition given in equation 1.47 and the correct choice of Φ, the wavelength of the dispersive wave can be estimated. In chapter 3 equation 1.47 is solved with the terms 1.48, 1.49 and 1.51 and the result is compared to the measurements.

Chapter 2

Experimental System

This chapter starts with section 2.1 giving a brief overview of the complex system placed at the Max-Planck-Institute of Quantum Optics that delivers the laser beam that is used for spectral broadening. It starts with an oscillator generating a beam that undergoes several amplification stages. It results in a 2 µm laser beam. This light can be sent to three different systems. One of them is the already existing synthesizer that needs it for spectral broadening. Another setup is the hollow core fibre (HCF) system built up for this thesis with the purpose of super continuum generation and spectral characterization of which. This will be described in more detail in section 2.2.

2.1 Light Source

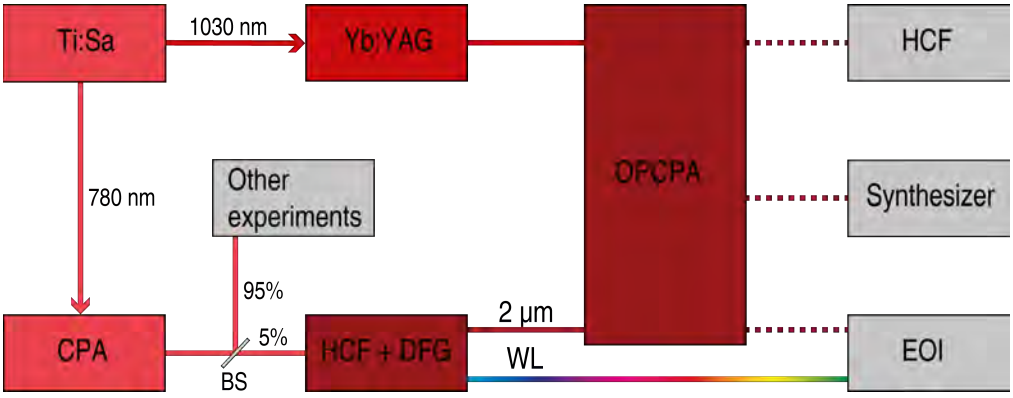

Figure 2.1: Schematic overview of the laser system delivering the 2 µm beam used for spectral broadening.

The first stage of the laser system, which is illustrated in figure 2.1, is a commercial Ti:Sapphire oscillator (Femtolasers, Rainbow II). The output pulse

train has a repetition rate of 78 MHz and a pulse energy of 3.5 nJ. Most of the energy is contained in a spectral region around 780 nm, only a very small part in the remaining spectrum that goes up to 1030 nm. The 780 nm light is sent as a seed to a multi-pass amplifier, based on Chirped Pulse Amplification (CPA). The output pulse energy of this amplifier is 0.8 mJ with a repetition rate of 3 kHz. Only 5 % of the beam is sent to a HCF for spectral broadening, the rest is used in other experiments. The HCF is 30 cm long and is filled with Krypton at 2.3 bar. The resulting white light is temporally compressed by pairs of chirped mirrors and then sent to a beta barium borate (BBO) crystal for intra pulse difference frequency generation (DFG). This NIR light is centred at 2 µm and is the seed for the following amplifier, which is based on optical parametric chirped pulse amplification (OPCPA) [14]. Due to DFG, the generated beam is also CEP stable. The residual white light passing the DFG process is sent directly to an experimental system. The necessary pump beam to amplify the 2 µm light inside the OPCPA originates from the 1030 nm light coming from the oscillator. This portion of light is sent to a regenerative thin disk Ytterbium-doped Yttrium Aluminium Garnet (Yb:YAG) amplifier [15]. This amplifier creates the pump beam with 16 mJ pulse energy at 3 kHz repetition rate for the OPCPA process.

The 2 µm that enters the OPCPA goes first to an acousto-optic programmable dispersive filter (Dazzler, Fastlite). With that device, the CEP of the diffracted beam can be changed as well as the phase up to several higher orders. This beam is then used as a seed for the OPCPA. This amplifier consist of two stages. The first stage is built up by a periodically poled lithium niobate (PPLN) crystal. 20 % of the pump beam is sent to this stage. The other 80 % can be sent to the scond stage, which is built up by two BBO crystals. The final pulse can contain an energy of up to 1 mJ and is only 15 fs short. It is also possible to send less pump power to the second stage, thus reducing the power of the amplified NIR beam. This is necessary for this thesis, as one goal is to characterize the spectral broadening generated by a beam that has only 80 µJ pulse energy.

The NIR light can be sent to three different systems. One of them gives the opportunity to measure not only the electric field of a light pulse in time but also in space. Since the working principle is based on electro optic sampling (EOS), the system is called electro optic imaging (EOI) [16]. For this thesis, the NIR pulse was measured just in time by using this system. For that, the 2 µm beam and the residual white light as a sampling pulse were sent to the EOI setup. The measured pulse is shown in figure 2.2, alongside the spectrum that was achieved through a Fourier transform of the electric field.

The beam can also be sent to the already existing optical waveform synthesizer [17]. The name of this device has the origin in the fact that a beam, spectrally broadened in a HCF, is split up into three different channels. Each of them covers another spectral region and is compressed by its own set of chirped mirrors. The channels are combined, so synthesized, at the end, delivering an

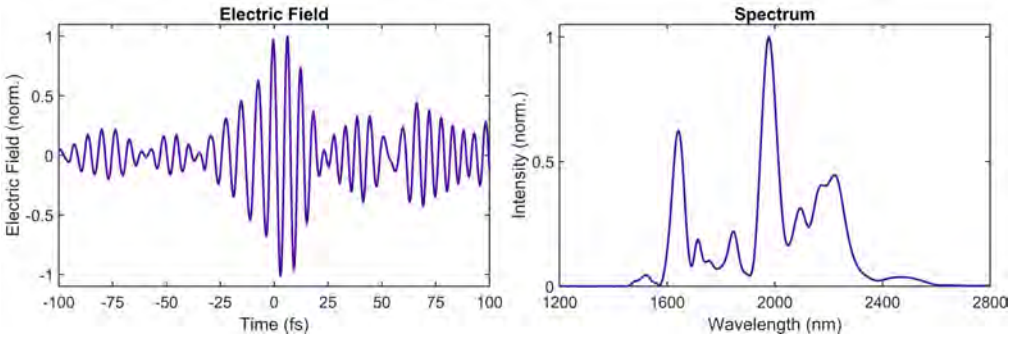

Figure 2.2: The electric field obtained by EOS of the 2 µm beam used for spectral broadening. The spectrum is calculated by a Fourier transformation of the electric field.

ultra short pulse having an ultra broadband spectrum spanning from less than 300 nm to above 3000 nm. The broadening happens in a HCF which is 30 cm long. The gas is air at atmospheric pressure and the full power of the OPCAP is used, so a pulse energy of 1 mJ. A HCF is also used for super continuum generation of the next generation synthesizer. The setup which is able to generate and measure a comparable super continuum by using less pulse energy, namely 80 µJ, is is the topic of the next section.

2.2 Spectral Broadening Setup

The system for spectral broadening consists of two parts. The first part, shown in figure 2.3, focuses on focusing the beam into the fibre as well as the fibre itself. The second part is for measuring the generated spectrum. In order to focus the beam, it is necessary to determine the required focus size. By assuming that the incoming beam is described through a fundamental Gaussian mode TEM_{00} and that the beam inside the fibre is a fundamental hybrid mode EH_{11}, the necessary beam waist is given by $w = 0.65a$, where a is the core radius of the fibre [18]. For a core diameter of 200 µm, the necessary beam diameter is $2w = 130$ µm. The measured gaussian beam diameter, obtained from a CMOS camera (Cinogy CinCam CMOS-1202), was $w = 93$ µm. Since the upper wavelength limit for that camera is 1320 nm, two photon absorption was assumed. This happened for the reason that the spectrum of the input beam starts at around 1600 nm, as it can be seen in figure 2.2. So a correction factor of $\sqrt{2}$ has to be multiplied, which results in the beam diameter being $2w = 131$ µm. Focusing was done by a pair of curved silver mirrors in front of the fibre. To improve the stability of the broadening process, a beam positioning system, including two motorized mirrors and two detectors, was installed (TEM μaligna). A wire grid polarizer

was placed in the beam path to clean the polarization of the beam going to the fibre. In addition to that, a 10 mm thick piece of Sapphire was added to compress the puls. Furthermore, the the acousto-optic modulator of the OPCPA was used to fine tune the dispersion of the pulse with the goal to improve the compression and therefore spectral broadening.

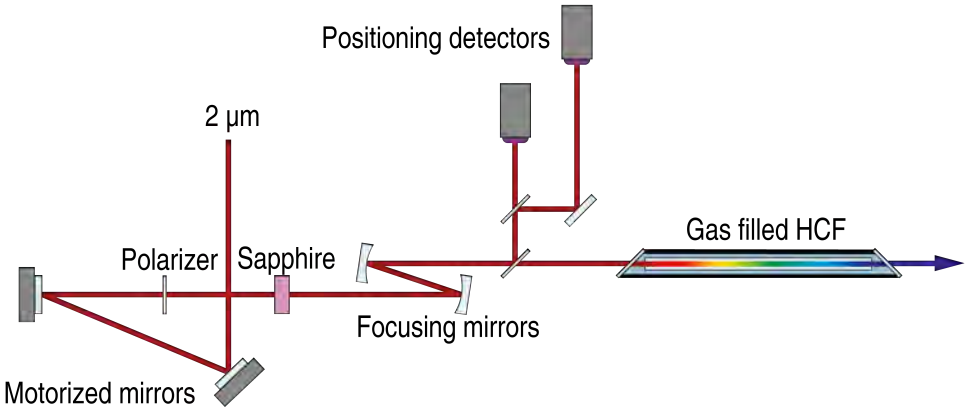

Figure 2.3: Layout of the system used for spectral broadening. A 2 µm beam with positioning stabilization is focussed into a gas filled HCF. The polarizer cleans the polarization of the beam and the Sapphire compresses the pulse in time.

The HCF was put in a V-grove holder. This holder lies in a vacuum tube that can be filled with different gases at different pressures. The entrance and exit windows are made out of 1 mm thick magnesium fluoride. The length of the fibre was chosen to be 30 cm, the same as for the existing synthesizer. The core diameter was reduced from 250 µm to 200 µm. The reason for that was to increase the peak intensity, and thus broadening, since the pulse energy of 80 µJ for the new synthesizer is less than the 1 mJ used for the already existing one. To additionally increase the broadening, the tube and so the fibre was filled with Argon or Krypton at different pressures.

The second part of the system deals with measuring the generated supercontinuum. The measurement happened in two different ways, called method A and B. This is shown in figure 2.4. Both have in common that a moveable thermal power meter (Thorlabs S401C) was installed so that the transmitted power can be acquired. An iris was put in the beam path to cut off the outer part of the beam. Since the spectrum for the current synthesizer ranges at least from 300 nm to 3000 nm, two spectrometers were needed to capture nearly the whole spectrum. The two used spectrometers are a VIS & UV spectrometer (OceanInsight, HDX) covering a range from 200 nm to 1000 nm and a NIR spectrometer

(OceanInsight, NIRQuest) for the wavelengths from 1000 nm to 2500 nm. To combine the spectra from the two devices into a single full range spectrum, an additional calibration setup was needed. This is described in the end of this section. To attenuate the beam coming out of the fibre, it was reflected by glass wedges. The difference between these methods is, that for method A the divergent beam was just attenuated and sent to the spectrometers. For method B, the outcoming beam was imaged onto the spectrometers by using a curved UV enhanced aluminium mirror. The advantage of method A is that the reflectivity of the wedges should not change much across the whole spectrum, whereas for method B the spectrum can be changed due to the reflectance at the aluminium mirror. The advantage of method B is that the measurement can be more stable since the output of the fibre is imaged at the spectrometer entrance, whereas for method A the divergent beam is entering the spectrometer.

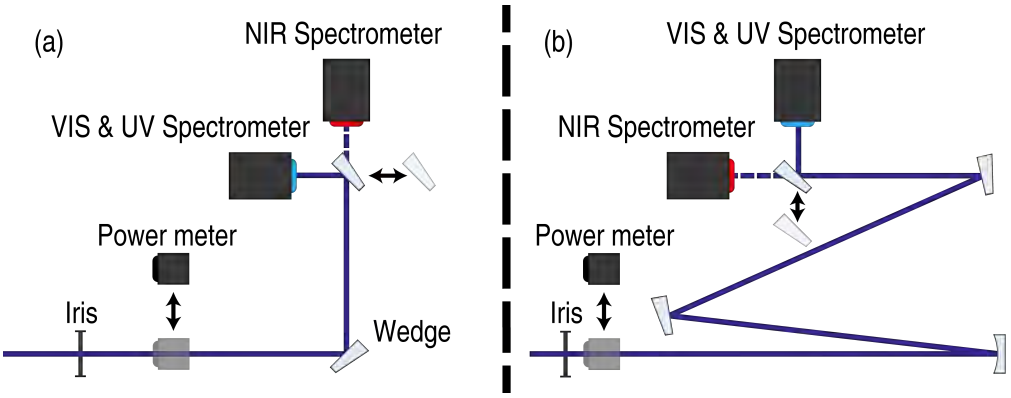

Figure 2.4: The two methods A and B for measuring the generated spectrum. (a) For method A the divergent beam is sent directly to the spectrometers, where one glass wedge can be moved to send the beam to either one of them. (b) For method B the output of the fibre is imaged onto the spectrometers by using a curved mirror. Both setups use glass wedges for attenuation, a power meter for transmission acquisition and an iris to let only the central part of the beam pass.

In order to combine the two single spectra captured by the two different spectrometers, an additional setup was needed to match them so that the measured intensity given by one spectrometer is comparable to the intensity of the other one. The system is shown in figure 2.5. The aim is to measure the powers contained in small spectral regions across the whole spectrum. From this, a spectrum can be obtained where the amplitude is determined by the readout of the power meter. Then, the complete spectrum is measured with each of the spectrometers. The resulting two spectra are finally fitted to the power spectrum, which makes a combination of the following individual spectra into

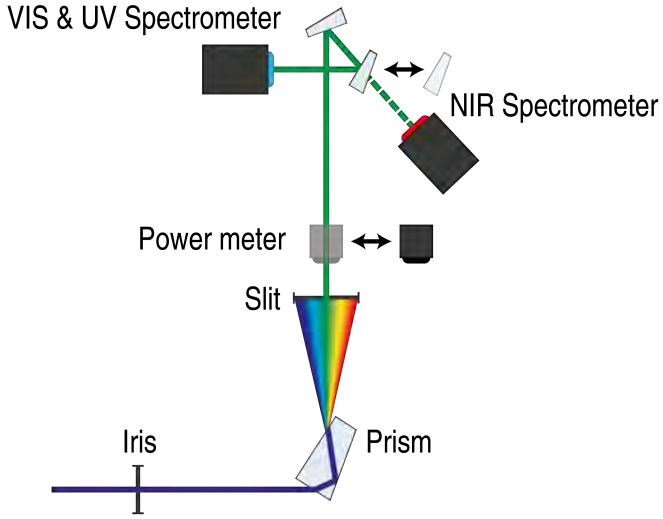

Figure 2.5: Setup used to match both spectrometers. A Pellin-Broca prism disperses the beam so that the power that is contained in a small spectral region can be measured.

one ranging from 200 nm to 2500 nm possible. This procedure requires that the beam is split up in a way that only a small spectral part can be measured. This happens by a Pellin-Broca prism (Thorlabs ADBU-20). The special geometry of this prism redirects one wavelength of the dispersed light beam in a 90° angle compared to the input beam, whereas the incoming angle defines that specific wavelength. So by rotating the prism, the wavelength that is deflected by 90° can be chosen. An additional slit narrows the spectral region that is metered by both the spectrometers and the power meter. To get the needed power spectrum, the prism is rotated step by step and each time the spectrometers are used to determine the spectral range and the power meter to obtain the contained power. From that, the power spectrum for matching the two spectrometers can be calculated.

Chapter 3

Characterization of Spectra

In this chapter, the acquired spectra are analysed. By using the measuring techniques described in the last chapter, namely method A and B in figure 2.4, six measurement series were performed. For both Argon and Krypton, the pressure and the input pulse energy were varied separately. For the pressure scan, the supercontinua were captured according to both methods. The spectra of the energy scan were only recorded with method A. The analysis starts with the pressure scan and continues with the energy scan.

3.1 Pressure Scan

The pressure scan was done by the two different methods. The pressure range was 0.8 bar to 3 bar for Argon and 0.3 bar to 2 bar for Krypton. The pulse energy was set to 80 µJ to make an estimation of the spectrum used in the next generation synthesizer easier. Since the shape of the spectra taken with both methods are comparable, only spectra from method A are shown. Additionally, not every spectrum taken at every pressure step is shown to make a clear presentation of the data. Every spectrum, at every pressure step and from both methods, was however analysed when it came to determine the spectral position of peaks. To compare the output spectra with the input, the spectrum of the OPCPA was taken with the same NIR spectrometer that was used to measure the supercontinua and is plotted in figure 3.1.

3.1.1 Argon

Before looking at the spectra, it should be checked that neither self focusing nor ionization is happening, as both processes can influence supercontinuum generation. If a Gaussian pulse shape is assumed, the resulting peak power of the input pulse is:

$$P_0 = 0.94 \cdot \frac{80\,\mu\text{J}}{15\,\text{fs}} = 5\,\text{GW}. \tag{3.1}$$

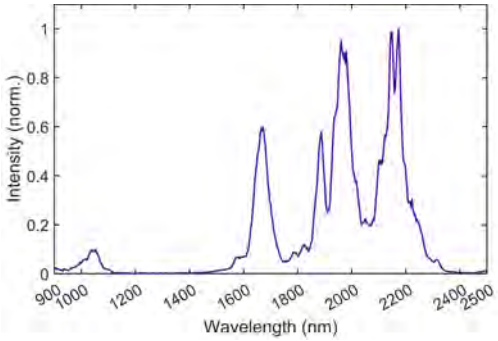

Figure 3.1: The spectrum of the input pulse coming from the OPCPA obtained using the same spectrometer that was used to measure the NIR part of the generated supercontinua.

According to 1.39, the critical power for self focussing at maximum pressure is:

$$P^{sf}_{cr,Argon} = \frac{\pi \cdot (0.61)^2 \cdot (2000\,\mathrm{nm})^2}{8 \cdot (1.0008) \cdot (9.4 \times 10^{-24}\mathrm{m}^2/(\mathrm{W} \cdot \mathrm{bar})) \cdot 3\,\mathrm{bar}} = 20\,\mathrm{GW}. \tag{3.2}$$

A critical power for ionization can be estimated by considering the over the barrier ionization intensity. This intensity marks the threshold where the electric field of the laser pulse is strong enough to lower the atomic potential barrier so far that the electron can escape classically [11]. With the relationship $P_{crit} = I_{crit}A_{eff}$, where $A_{eff} = 0.48\pi a^2$ is the effective mode area from chapter 1 and I_{crit} the critical intensity, the critical power for above barrier ionization is given by:

$$P^{ion}_{cr} = 4 \times 10^{13} \cdot (I_p[\mathrm{eV}])^4 \mathrm{W/m}^2 \cdot A_{eff}, \tag{3.3}$$

with I_p the ionization potential from table 1.1. This results for the critical ionization power of Argon to be

$$P^{ion}_{cr,Argon} = 4 \times 10^{13} \cdot (15.76)^4 \mathrm{W/m}^2 \cdot 0.48 \cdot \pi \cdot (100\,\mu\mathrm{m})^2 = 37\,\mathrm{GW}. \tag{3.4}$$

These two critical powers are greater than the pulse peak power, so the corresponding effects can be neglected at first. It should be noted though that the peak power can increase as the pulse experiences self compression and ionization can happen at even lower intensities due to tunnel ionization [19]. Ionization by tunnelling can happen earlier as the potential barrier is again lowered due to the laser pulse, but only as much as quantum mechanical tunnelling can cause electrons to escape the potential.

The evaluation of the spectra starts with figure 3.2, where three spectra for broadening in Argon at the lower pressure range are shown. In comparison with the input spectrum, broadening is clearly visible. The spectrum is extended in both the longer and shorter wavelength regime. This is due to the intensity

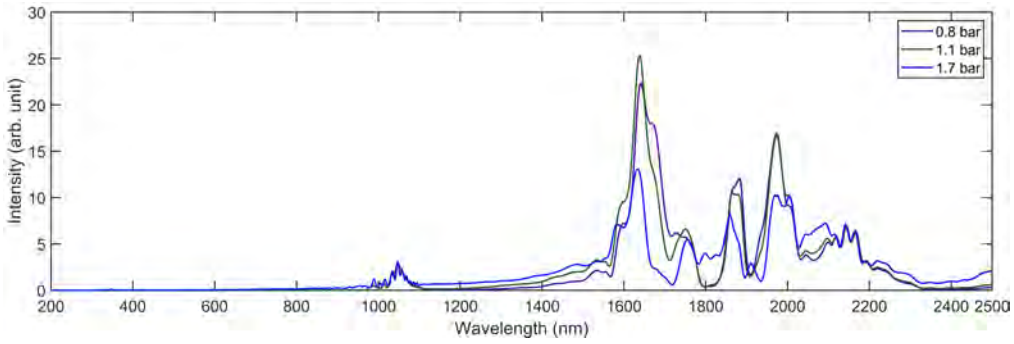

Figure 3.2: Spectra for broadening in Argon from 0.8 bar to 1.7 bar.

dependent nonlinear refractive index and thus a result of SPM and self steepening. The fringes close to 1000 nm arise from interferences of the broadened spectrum and residual light coming from the OPCPA. Since the strength of spectral broadening depends on the nonlinear parameter, which is linearly pressure dependent, the broadening increases as the pressure does. This can be seen in figure 3.3, where spectra at higher Argon pressures are shown. The broadening

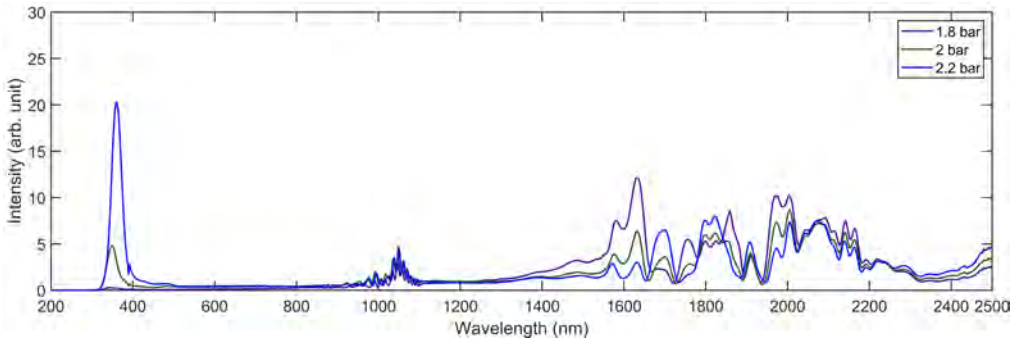

Figure 3.3: Spectra for broadening in Argon from 1.8 bar to 2.2 bar.

gets stronger as the pressure increases, now reaching the VIS region of light and the UV. In parallel, the intensity of longer wavelengths is intensified. At the same time, the NIR part of the input pulse is altered due to SPM and self steepening, leading to a decreased spectral intensity and an additional spectral reshaping. Starting from 1.8 bar, the spectrum also starts to have another new spectral feature, a resonant dispersive wave in the UV. A prerequisite for this is that the input pulse lies in the anomalous dispersion region of the Argon filled fibre. To verify this, the spectrum at 2.2 bar and the corresponding GVD curve are plotted in figure 3.4, alongside the ZDW for the full pressure range.

It can be taken from this figure that the input spectrum is indeed in the

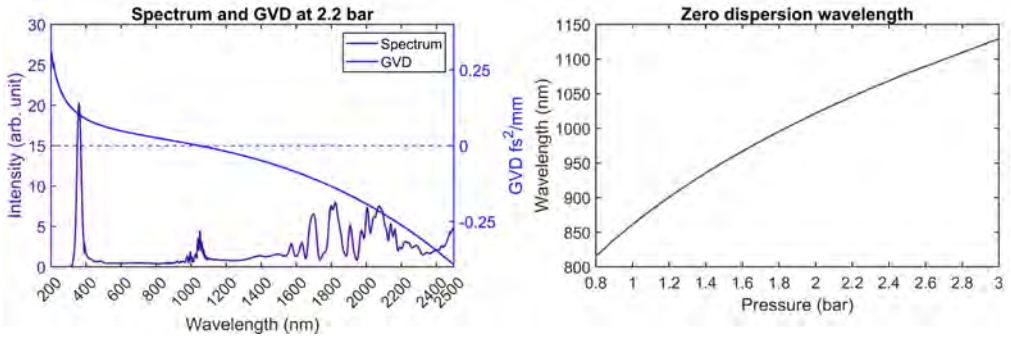

Figure 3.4: On the left is the spectrum for broadening in Argon at 2.2 bar with the associated GVD curve. On the right is the ZDW for the entire pressure range of the scan performed with Argon.

anomalous spectral region of the HCF and the newly created wave is in the normal dispersion regime, hence the name dispersive wave. It is also shown that the ZDW is always smaller than the lowest wavelength of the input spectrum, the pulse is located within the anomalous dispersion region for the entire pressure range. To further confirm the presence of a dispersive wave, the characteristic length scales, that give an estimation after which distance effects due to dispersion and nonlinear interaction occur, as well as the soliton order of the input pulse, are shown in figure 3.5. It is no surprise that the nonlinear length is

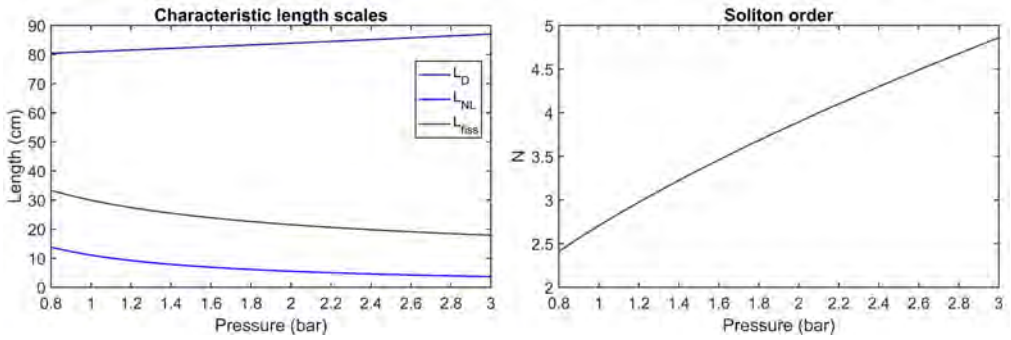

Figure 3.5: The left figure shows the dispersion, fission and nonlinear length as introduced in chapter 1.4 in the case of an Argon filled HCF. On the right hand side the related soliton order is plotted.

smaller than the fibre length of 30 cm for every pressure, since there is spectral broadening on every shown spectrum. Additionally, the stronger broadening with increasing pressure is reflected by the the negative slope of the nonlinear length curve. The positive slope of the dispersion length curve however is ex-

plained by the position of the ZDW, as it comes closer to the input pulse and thus reduces the absolute value of the GVD at the center wavelength. In section 1.4.2 it was mentioned that a soliton order of $N > 1$ is necessary for the build up of a RDW. This condition is fulfilled in this case as the nonlinear length is smaller than the linear length. If both lengths were equal, the soliton order would be $N = 1$, and the pulse would propagate through the fibre without any change. But since the nonlinear length is smaller, the input pulse starts with being spectrally broadened by SPM in the beginning of propagation. Then compression through the anomalous dispersion of the fibre follows. This interplay goes on and on, producing a shorter and more broadband pulse than at the input. The higher order dispersion is then responsible for the pulse to break up at some point. This specific point is described by the fission length and it is also plotted in figure 3.5. At 1 bar, the fission length reaches 30 cm and goes down to 18 cm at 3 bar. The increasing spectral intensity of the RDW in figure 3.3 can be explained by the fact that the fission point moves towards the fibre entrance. For the lower pressure range, the point of fission is behind the fibre exit, leading only to a limited transfer of energy to the RDW. A prerequisite for the build up of a dispersive wave is that the spectrum is broadened enough to reach the wavelength of the dispersive wave. If the spectrum is not broadened enough before the fibre ends, there will not be a RDW. For an increasing pressure, the point of fission moves towards the fibre input. This means an increase in the length over which the energy transfer to the dispersive wave happens, as the beginning of the build up also starts earlier. The maximum resonant energy transfer can be reached if the fission happens at the output of the fibre or before. A point close to this is reached at 3 bar, as it can be seen in figure 3.6. The spectrum

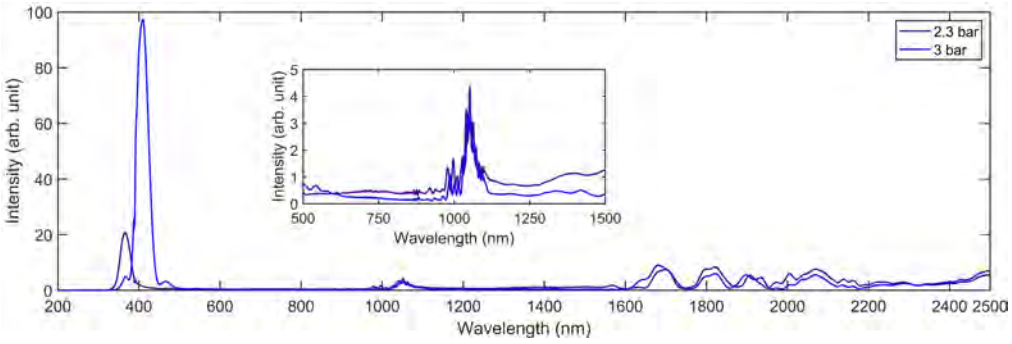

Figure 3.6: Spectra for broadening in Argon from 2.3 bar to 3 bar. The inset shows the spectrum in the region from 500 nm to 1500 nm to highlight the reduced overall broadening at higher pressures.

at 3 bar shows a strong RDW. Although this alone is not a sign for fission, the broadened spectrum between the input pulse and the RDW is weaker than for lower pressure. This is shown in the inset of figure 3.6. This is indeed a sign

that the fission happened inside the fibre, as only the higher order input soliton can support a broadband spectrum that reaches the wavelength of a RDW. But after the break up, the remaining solitons can not support the broad spectrum, which results in a decrease of spectral intensity of the broadened part. Fission happens inside of the fibre for pressures between 2.3 bar and 3 bar according to the measurements. The calculated fission length moves from 20 cm to 18 cm for these pressures, so the calculated values are smaller than the real fission length.

The wavelength of the RDW can be estimated by using the equation for phasematching 1.47, given in section 1.4.2. Solving for the wavelength happened by using the different phase terms 1.48, 1.49 and 1.51. The measured wavelengths of the RDW, form both methods A and B, as well as the results from solving the phasematching condition, are illustrated in figure 3.7. The

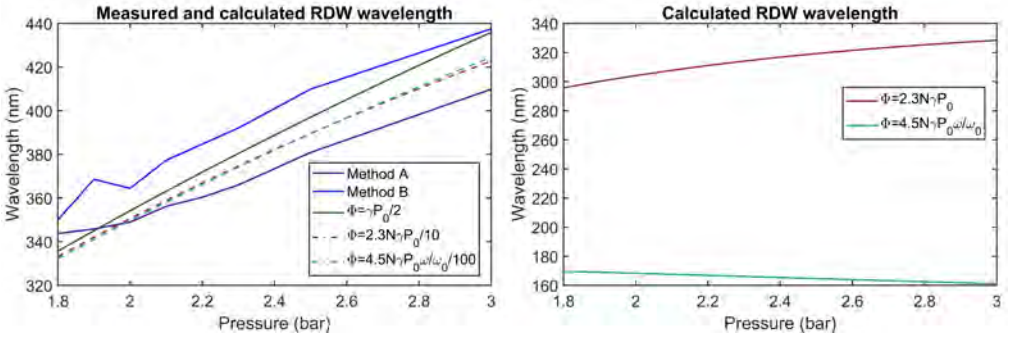

Figure 3.7: On the right, the RDW wavelength is plotted when the terms 1.49 and 1.51 are used in the phase matching condition for an Argon filled HCF. On the left, the measured RDW position is shown from both methods A and B, as well as the result from solving the phase matching condition. For that, term 1.48 and by correction factors multiplied terms 1.49 and 1.51 were used.

first thing to notice is the offset of 20 nm $\sim$ 30 nm between both measurement series. This is originating from the varying input power from the OPCPA, as the measurements were done on two different days. The second thing to notice is that only the phase term $\gamma P_0/2$ gives promising results. The other two terms, $2.3N\gamma P_0$ and $4.5N\gamma P_0\omega/\omega_0$, give wavelengths that are considerably off as it can be seen from the right hand side of figure 3.7. The second term even predicts a decrease of the wavelength with increasing pressure. This however can be changed by multiplying 1/10 with the first term and 1/100 with the second term. The predicted RDW wavelength is then much closer to the measured values. The magnitude of the slopes also become larger, which seems to better fit to the measured curves. The origin of these correction factors can be understood by looking at the change of the absolute values of the phase terms due to the approximations done. In the first approximated term, the nonlinear coefficient and the peak power γP_0 is multiplied by $2.3N$ in order to take account for self

compression. From figure 3.5 it can be seen that the soliton order is something around 4. This leads to a factor of $2.3 \cdot 4 = 9.2$ that γP_0 is multiplied with. As a result, by correcting the whole phase term by a factor of 1/10, the contribution from the approximation is nearly compensated. This is the same for the other phase term. Here, γP_0 is multiplied by $4.5N\omega/\omega_0$. This approximation includes besides of self compression also the shock term. By assuming a wavelength of 400 nm for the dispersive wave and 2000 nm for the input soliton, the shock term has the value of 5. By again taking 4 as the soliton order, the factor becomes $4.5 \cdot 4 \cdot 5 = 90$. Once again, the needed correction factor, which is 1/100 in this case, compensates the contribution originating from the approximations. This is no surprise, as the only phase term that gives good results without further correction is $\gamma P_0/2$, which is already close to γP_0. The necessity of these new factors is although not yet clear, since these approximations were actually done to improve the predictability of the RDW wavelength. But as it seems is the influence on the phasematching condition too strong. One explanation can be that the power of the compressed pulse is not as high as it is expected. This can result from the power transmission of $\sim 45\%$, which was both measured as well as calculated using the attenuation constant from equation 1.25. So even though the pulse is compressed, the energy loss of the pulse is reducing the peak power. In addition, the contribution from the negative dispersion can be smaller than expected, which would lead to a longer soliton pulse in time, what would again reduce the peak power used in the approximations. In the following subsection, the gas is exchanged by Krypton and it will be examined if these corrections are needed again.

3.1.2 Krypton

Like in the case for Argon, it should be first checked that effects arising from ionisation or self focusing are not too strong. The peak power of $P_0 = 5\,\mathrm{GW}$ stays the same, the critical powers for self focusing as well as for above barrier suppression ionisation take the following new values:

$$P^{sf}_{cr,Krypton} = \frac{\pi \cdot (0.61)^2 \cdot (2000\,\mathrm{nm})^2}{8 \cdot (1.0011) \cdot (26.3 \times 10^{-24}\mathrm{m}^2/(\mathrm{W} \cdot \mathrm{bar})) \cdot 2\,\mathrm{bar}} = 11\,\mathrm{GW}, \quad (3.5)$$

and

$$P^{ion}_{cr,Krypton} = 4 \times 10^{13} \cdot (14)^4 \mathrm{W/m}^2 \cdot 0.48 \cdot \pi \cdot (100\,\mu\mathrm{m})^2 = 23\,\mathrm{GW}. \quad (3.6)$$

Once again are the critical powers larger than the peak power at the input. But since the nonlinear refractive index is larger for Krypton than for Argon, the values of these powers are smaller and thus closer to the peak power of the pulse. The difference in the absolute value of the nonlinear refractive indices also shows in the pressure scan done for Krypton. The first spectra at low pressures, where no dispersive wave is appearing, are shown in figure 3.8. Here,

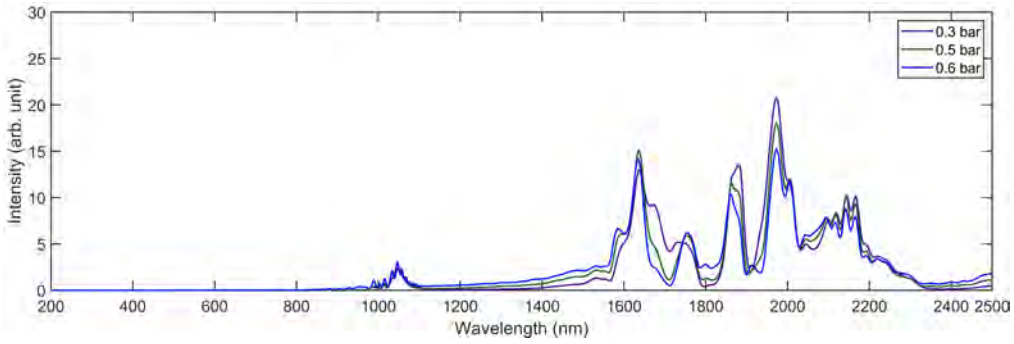

Figure 3.8: Spectra for broadening in Krypton from 0.3 bar to 0.6 bar.

the same behaviour can be observed as for Argon, namely that for increasing pressure the broadening due to SPM gets stronger. As the nonlinear refractive index for Krypton is roughly three times larger than for Argon, see table 1.1, it is no surprise that the pressure is three times smaller than for Argon to get comparable results. This comes from the fact that for the different phenomena the product of nonlinear refractive index and pressure is a measure for the strength of the process. The fringes close to 1000 nm are again interferences between broadened light and residual light coming from the OPCPA. If the pressure is increased, a dispersive wave is emerging. This is shown in figure 3.9. The broadened spectrum with its GVD curve, as well as the ZDW for

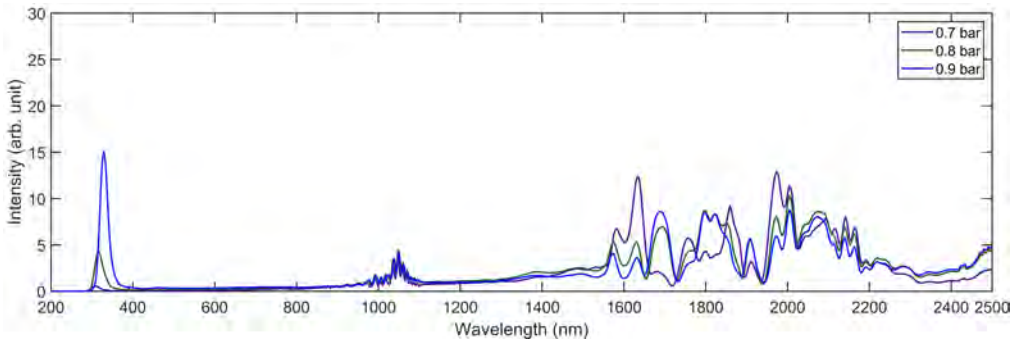

Figure 3.9: Spectra for broadening in Krypton from 0.7 bar to 0.9 bar.

the whole pressure range, is shown in figure 3.10. As expected is the input pulse in the anomalopus dispersive region of the fibre, thus making it possible to create a RDW. Also the ZDW is always smaller than the input spectrum for every pressure within the scanning range. The position of the RDW is shifted to higher wavelengths with increasing pressure in addition to an increase in spectral amplitude, what can be seen in figure 3.9. This behaviour was already seen in

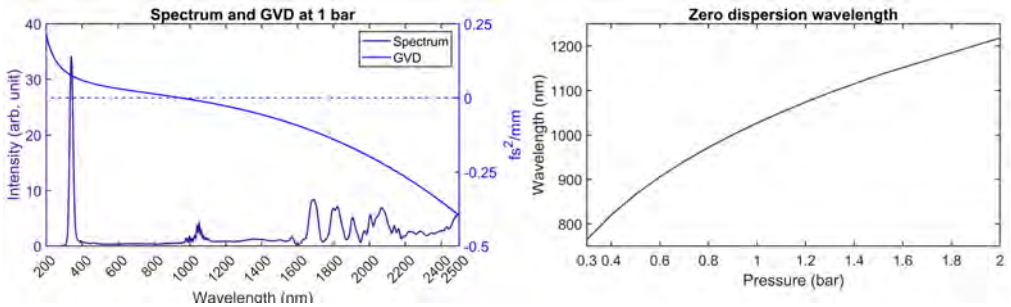

Figure 3.10: On the left is the spectrum for broadening in Krypton at 1 bar with the associated GVD curve. On the right, there is the ZDW for the entire pressure range of this scan.

the case of Argon, hence why the characteristic length scales for Krypton, shown in figure 3.11, are comparable with the length scales in figure 3.5 for Argon. The

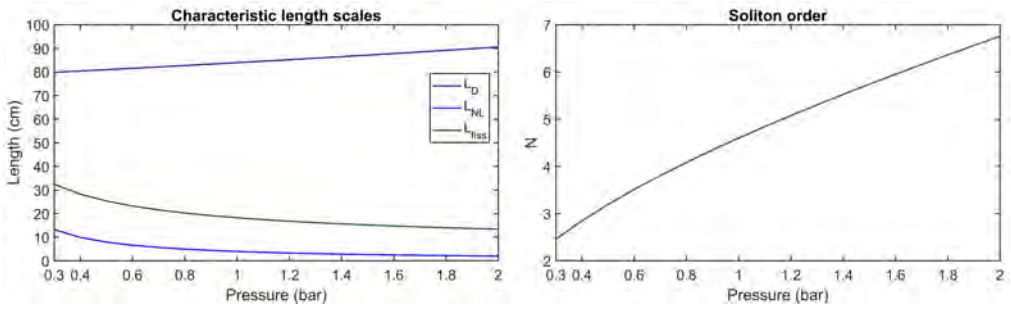

Figure 3.11: The left figure shows the dispersion, fission and nonlinear length for a Krypton filled HCF. On the right hand side the related soliton order is plotted.

length scales show the same behaviour. The nonlinear length is smaller than the dispersion length, leading to a soliton order larger than one. This is a prerequisite for the RDW generation, as the soliton broadens spectrally till the UV region where a resonant transfer of energy can happen. The soliton order also increases as the pressure does, reaching even higher values than in the case for Argon. This results from the nonlinear length reaching values that are even lower. But the soliton order is still smaller than 15, such that modulation instabilities should not occur [20].

After a sufficient propagation distance, the soliton will undergo fission and break up. For Argon, fission happened around 3 bar inside the fibre. This would result in fission inside the fibre at around 1 bar for Krypton. This is indeed true, as it can be seen in figure 3.12.

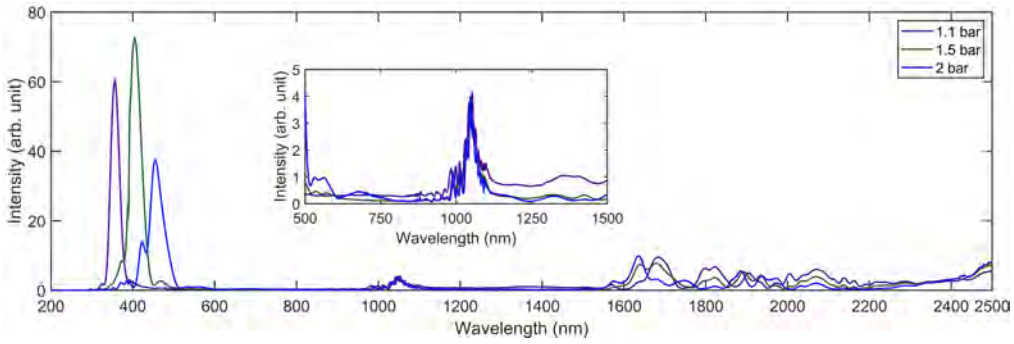

Figure 3.12: Spectra for broadening in Krypton from 1.1 bar to 2 bar. The inset shows the spectrum in the region from 500 nm to 1500 nm to highlight the reduced overall broadening at higher pressures.

Here, the amplitude of the RDW does not increase anymore. This is the case if the fission happens before the end of the fibre, as after this event the energy transfer stops and thus the spectral amplitude will not increase any longer. By further increasing the pressure, the fission point just moves away from the end of the fibre towards the input. Like it happened in the case for Argon, the overall broadening also starts to decrease once the fission happened. This can be seen in the inset of figure 3.12. But unlike before, the RDW shows an interesting shape after the fission happened. At lower pressures, where no fission happened yet, the the RDW is spectrally a clear pulses with one maximum and strictly monotonous slopes. But after the fission, the dispersive waves gets spectral wings. These wings become stronger with propagation distance, as for increasing pressure the distance between fibre output and point of fission gets larger. The dispersive waves, that are more broadband with these side wings, are shown in figure 3.13.

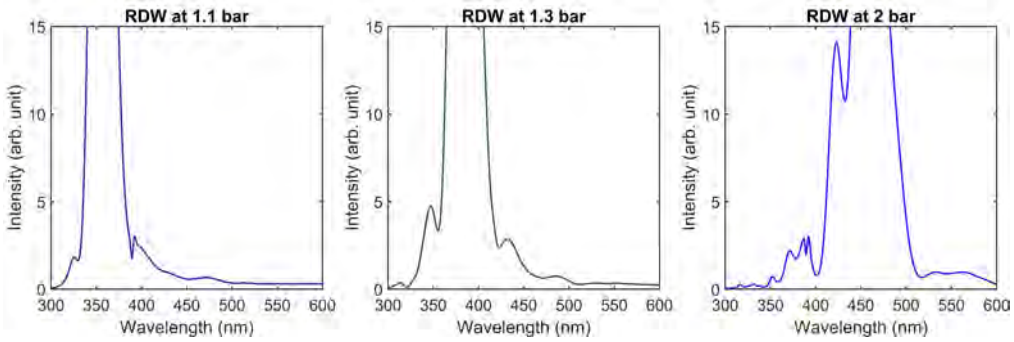

Figure 3.13: The spectral wings of the RDW for different Krypton pressures.

Since the dispersive wave can be considered to be a pulse propagating on its own, it can experience both linear and nonlinear interaction with the gas filled HCF. Whereas the linear part causes the pulse to disperse, the nonlinear part can also influence the pulse in the same way as the input pulse. Since the spectrum is more broadband and has spectral wings, it shall be roughly examined if a nonlinear process like SPM can be the reason for this spectral shape. The RDW could experience this in two ways. Firstly, this can happen by cross phase modulation (XPM). Here, the high intensity of the NIR pulse changes the refractive index by the means of the Kerr effect. Whereas this is responsible for the main pulse to get broadened, also the RDW sees this intensity dependent refractive index and gets affected [21]. Secondly, the intensity of the RDW itself could induce this effect on its own. This is the case if the RDW is propagating by itself after the fission happened and is lagging behind the main pulse as the linear refractive index is higher for shorter wavelengths. This means that the high intensity of the RDW alone could cause SPM to broaden its spectrum [22], [23]. To roughly check if this is a possibility, the following approximations are done. The central wavelength of the RDW is 400 nm with the bandwidth of 20 nm. The conversion efficiency from the soliton input pulse energy to the RDW is 20 %. For that, the numerically calculated area of the dispersive wave is set in ratio the the area of the full spectrum with also accounting for the transmission efficiency of 45 %. The value of 20 % is herby reasonable since even higher values are possible [22], [23]. The RDW has then the following duration:

$$\tau^{RDW} = \frac{2 \cdot ln(2) \cdot (400\,\mathrm{nm})^2}{\pi \cdot c \cdot 20\,\mathrm{nm}} = 11.7\,\mathrm{fs}. \tag{3.7}$$

The dispersion that the pulse will experience, which would result in a longer time width of the pulse, is neglected for the sake of estimation. The resulting peak power would be

$$P_0^{RDW} = 0.94 \frac{0.2 \cdot 80\,\mu\mathrm{J}}{11.7\,\mathrm{fs}} = 1.3\,\mathrm{GW}. \tag{3.8}$$

The nonlinear coefficient is going to be

$$\gamma^{RDW} = \frac{36.7 \times 10^{-24}\mathrm{m}^2/(\mathrm{W} \cdot \mathrm{bar})) \cdot 2\,\mathrm{bar} \cdot 2}{400\,\mathrm{nm} \cdot 0.48 \cdot (100\,\mu\mathrm{m})^2} = 76.5 \times 10^{-9}\,\mathrm{m}^{-1}\mathrm{W}^{-1}, \tag{3.9}$$

with the nonlinear refractive index being corrected for the RDW wavelength that is smaller than the 2 µm used before. This results in the nonlinear length to be

$$L_{NL}^{RDW} = \frac{1}{\gamma^{RDW} \cdot P_0^{RDW}} = 1\,\mathrm{cm}. \tag{3.10}$$

This outcome means that the RDW gets spectrally broadened if the propagation distance is in the order of 1 cm. For that to happen, the fission has to occur at least one centimetre before the fibre ends. The calculated fission length for the

Krypton filled fibre goes from 18 cm at 1 bar to 13 cm at 2 bar. Even though the fission length is always smaller than the real length and thus not entirely correct, it is good enough to say that the RDW at 2 bar had a long enough travel distance inside the fibre to get spectrally broadened if the necessary travel distance is in the order of one centimeter. In any case, this is just an approximation, since at first the pulse would experience XPM, which then switches to be SPM as the pulse lags behind. Not only the Kerr contribution could explain the shape of the spectrum. Other effects arising form coupling to higher order fibre modes or ionization also have an influence on the spectrum in the UV. This will be mentioned in the next subsection, as the energy scan revealed a similar behaviour.

Now, the wavelength of the dispersive wave is analysed by comparing the measured values with the ones calculated by the phasematching condition 1.47. The general behaviour of the wavelength is the same as it was seen for Argon, but in the case for Krypton even lower wavelengths can be reached. The two phasematching terms that were corrected in order to fit the curves in the case of Argon are again corrected in the same way to see if the prediction is improved one more time. Figure 3.14 shows the measured and calculated wavelengths of the dispersive wave. Like in the case for Argon, only one not corrected

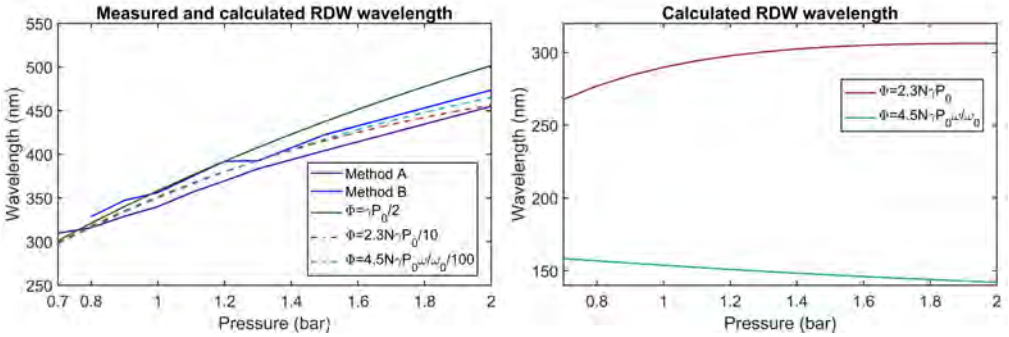

Figure 3.14: On the right, the RDW wavelength is plotted when the terms 1.49 and 1.51 are used in the phasematching condition for a Krypton filled fibre. On the left, the measured RDW position is shown from both methods A and B, as well as the result from solving the phase matching condition. For that, term 1.48, as well as the by correction factors multiplied terms 1.49 and 1.51, were used.

phasematching term gives results close to the measured values. The other two terms need an additional correction factor to get close to the measured data. Again, the same correction factors as they were used for Argon improve the results. But in contrast to the corrected curves shown in figure 3.7, the corrected curves here have a stronger curvature in comparison with the measurements. So, if the pressure range would be extended, it would probably result in an increasing

error of the predicted wavelength. Since the calculated results are worse than in the case for Argon, a possible explanation could be that ionization affects the phasematching condition [8], [24]. This would especially happen in the case of Krypton, as the ionization threshold is lower than for Argon. Although the input power is too low for significant above barrier suppression ionization, tunnel ionization can occur for even lower powers. But even if the power is not sufficient for barrier suppression ionization at the beginning, due to soliton self compression the critical power can be reached. In any case, a plasma origination from ionization would lead to an additional term in the phasematching condition [25]. This term could potentially improve the calculated results. But this could also result in a RDW in the IR region. However, this can not be verified as the covered wavelength region only goes up to 2500 nm with the used spectrometers and the new wave would be further in the IR.

A comparison of the RDW wavelengths of both gases show that the lowest values can be achieved with Krypton. This has an influence on the bandwidth of the broadened spectrum, as it is shown in figure 3.15. Here, the spectrum

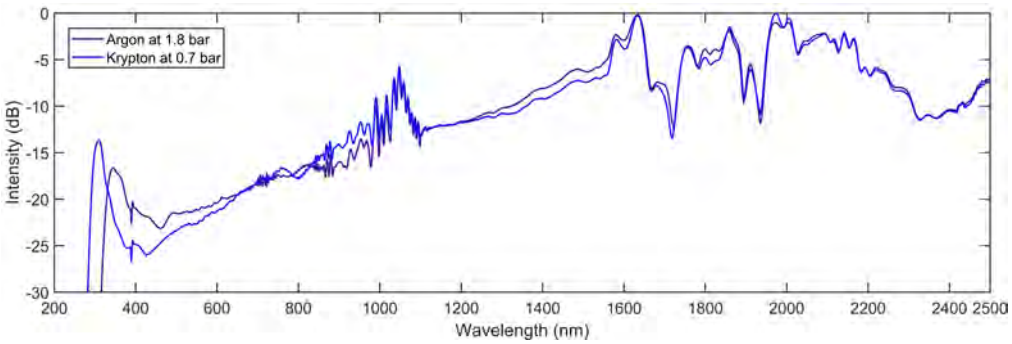

Figure 3.15: Comparison of broadening between the two gases. The pressures where chosen such that the RDW is weak, thus producing a flat overall spectrum.

obtained with Argon at 1.8 bar is plotted with the spectrum of Krypton at 0.7 bar. The pressures were chosen with the aim of having a flat spectrum. Therefore, the RDW is weak as it just started to build up at the fibre exit. This is of importance for the next generation synthesizer, as the goal is to produce a flat supercontinuum. The figure shows that a more broadband spectrum can be achieved with Krypton, which is a result of the resonant transfer of energy to the RDW wavelength that is shorter than for Argon. The broadening in the spectral region between the RDW and the input pulse is for both gases comparable, only for Argon it is a bit stronger.

3.2 Energy Scan

Besides a pressure scan, an additional input pulse energy scan was performed. This happened by changing the pump power of the OPCPA, which led to a varying power of the beam sent into the fibre. Like in the previous section, the energy of the pulse was varied for Argon and Krypton in different ranges, where the maximum energy was smaller in the case for Krypton as the nonlinearties are stronger. The pressure was kept constant for both gases at 1 bar. In common was the minimum energy at 80 µJ, which is the same pulse energy used in the pressure scan. The maximum value was 247 µJ for Argon and 147 µJ for Krypton.

3.2.1 Argon

It can be seen in figure 3.2 that for 80 µJ the pressure has to be increased above 1.7 bar to see a RDW emerging, below that pressure there is only broadening due to SPM and self steepening happening. This is the same case here, where the energy has to be increased up to 147 µJ in order to see a RDW. This is shown in figure 3.16. For lower pulse energies, there was broadening comparable to what was shown in the pressure scan. The peak power also stays below the critical powers calculated in section 3.1.1, even though it can be three times larger as the pulse energy is roughly increased by that factor during this scan. From the

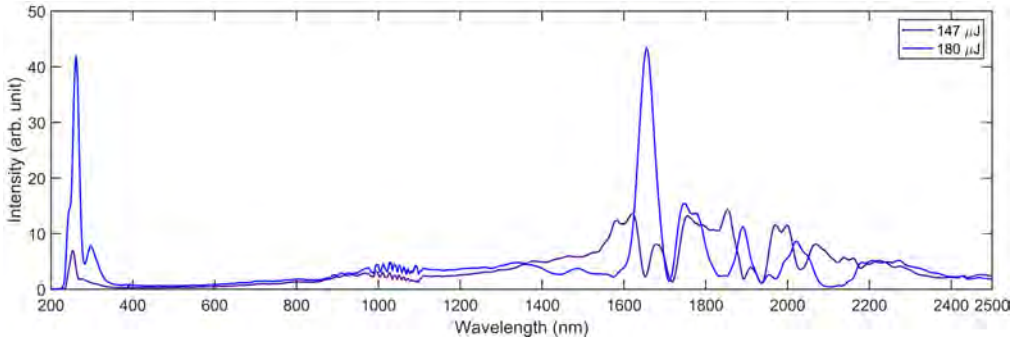

Figure 3.16: Spectra for broadening in Argon at 147 µJ and 180 µJ.

first two spectra, it can be seen that with increasing pulse energy the spectral amplitude of the dispersive wave grows. Again, this is a result of the fission length decreasing with pulse energy. This is illustrated in figure 3.17. The dispersion length is constant as it only depends on the absolute value of β_2 and the pulse width in time. The nonlinear length decreases, and so does the fission length. Like it could be seen in the pressure scan, a calculated fission length of about 20 cm seems to equal the length of the fibre. The soliton order is increasing and has comparable values to what was calculated for the pressure scan. An

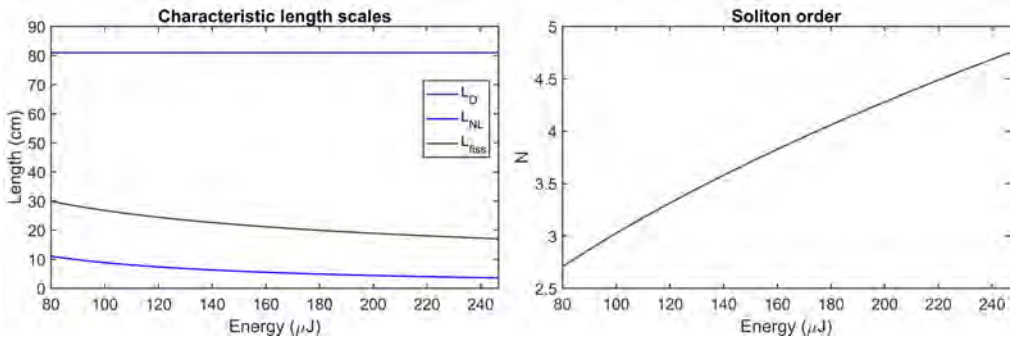

Figure 3.17: The left figure shows the dispersion, fission and nonlinear length for an Argon filled HCF. On the right hand side the related soliton order is plotted.

interesting observation of the measured spectra is that the wavelength of the RDW seems to increase a bit, which is in contrast to what the phasematching condition would predict. Whereas for increasing pressure the wavelength should become longer, an increase in pulse energy should lead to a shorter wavelength. So, the phasematching condition, given the different terms that account for the phase of the soliton, cannot predict the wavelength of the RDW for increasing pulse energy in a reliable way.

During the pressure scan for Krypton it could be seen that the dispersive wave gets more broadband and spectrally modulated with increasing pressure as soon as the fission happened. Something like this happens again if the pulse energy is increased, but in this case the modulations are even more pronounced. This is shown in figure 3.18. Here, the RDW shows spectral modulations that

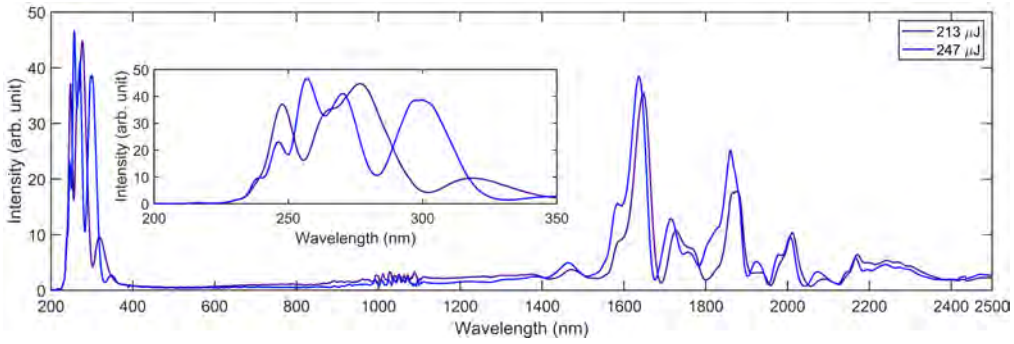

Figure 3.18: Spectra for broadening in Argon at 213 µJ and 247 µJ. The inset zooms to the spectral region of the dispersive waves.

were not seen before in this extent. Also, the total spectral bandwidth is larger

than in previous spectra, it is for example more broadband than the strong RDW in figure 3.6. Furthermore, the maximum spectral amplitude is lower than what was measured during the pressure scan. This is in contrast to the higher pulse energy of the input pulse, since one could assume that the dispersive wave also contains more energy, so leading to a larger spectral amplitude. A possible explanation is that XPM and SPM is reshaping the spectrum of the RDW. It was shown in the last section, that for an input pulse energy of 80 µJ and higher pressure, the short nonlinear length would allow SPM to affect the RDW after the fission point. The strength of this nonlinear process is determined by the product of pressure and pulse energy. During the pressure scan, the strongest RDW appeared at 3 bar and 80 µJ pulse energy. In this energy scan, the highest pulse energy is roughly three times larger than in the pressure scan. At the same time, the pressure is three times smaller. So the not changing product of energy and pressure can not alone explain the heavy modulation in this energy scan. A possible explanation for that could be that the conversion efficiency from the NIR to the RDW is not constant, it can increase with increasing input pulse energy [22], [23]. This would then lead to the situation that the power contained in this RDW is exponentially higher than during the pressure scan. Since the strength of SPM is then dependent on pressure, pulse energy and conversion efficiency, its effect can be stronger, what could explain why the spectrum of the RDW is now altered much more than before. Another reason could be that the output window is introducing SPM to the RDW. This would explain why it is happening during the energy scan and not the pressure scan, as the strength of SPM in the window does only depend on the pulse energy and no the pressure. But this should then also affect the NIR pulse, as even with high conversion efficiency most of the energy is still contained in this spectral part. Another explanation could be the that the fission length is so small that after the first fission occurred, the main pulse gets compressed again and thus creating an additional RDW at a wavelength close to it [26], [8]. Furthermore, higher order modes could now contain more energy, which would also result in additional spectral components around the RDW [27]. Moreover, plasma effects can not be excluded completely [24], [28], [29] as the impact of free electrons on the refractive index can also cause the modulations on the output spectrum. This would require ionization to happen, which is favoured by the higher peak power in this case and the fact that tunnel ionization happens at lower powers than barrier suppression ionization. Also the self compressing pulse can lead to more ionization due to a higher peak power.

3.2.2 Krypton

The maximum peak power of the input pulse is $P_0 = 9\,\mathrm{GW}$ for the maximum pulse energy of 147 µJ. This is lower than the critical power for self focusing of $P^{sf}_{cre,Krypton} = 22\,\mathrm{GW}$ and barrier suppression ionization $P^{ion}_{cr,Krypton} = 23\,\mathrm{GW}$. The first captured spectrum at 80 µJ has already a RDW, which is not surprising

as this combination of pressure and pulse energy was already part of the pressure scan in the last section. This spectrum is shown in figure 3.19. Like before, the

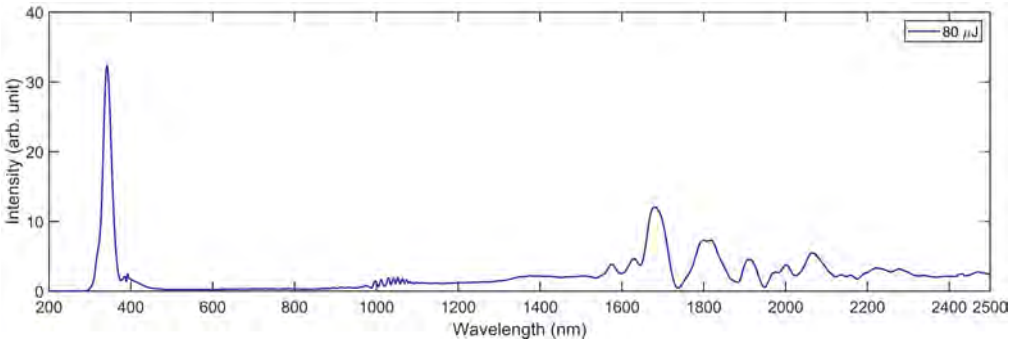

Figure 3.19: Spectrum for broadening in Krypton at 80 µJ.

NIR part is broadened and the RDW amplitude is strong. Since it was found out that the fission happens at the end of the fibre, at a pressure around 1 bar, it is no surprise that the calculated fission length is around 18 cm, as it can be seen in figure 3.20. With increasing pulse energy the nonlinear length decreases

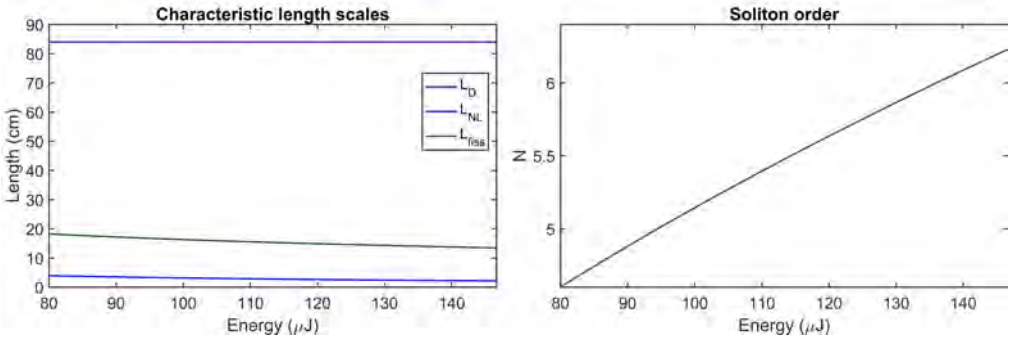

Figure 3.20: The left figure shows the dispersion, fission and nonlinear length for a Krypton filled HCF. On the right hand side the related soliton order is plotted.

and so the soliton order increases. The dispersion length stays again constant, as the pulse energy does not change. The characteristic length scales show the same behaviour as before, which is not surprising as the product of nonlinear refractive index, pressure and pulse energy is comparable to previous scans. If the pulse energy is further increased, the spectra as shown in figure 3.21 are generated. Once again, the dispersive wave gets spectrally broadened like in the case for the energy scan done with Argon. The spectrum also shows the same modulations, which suggests that the previously mentioned explanation of

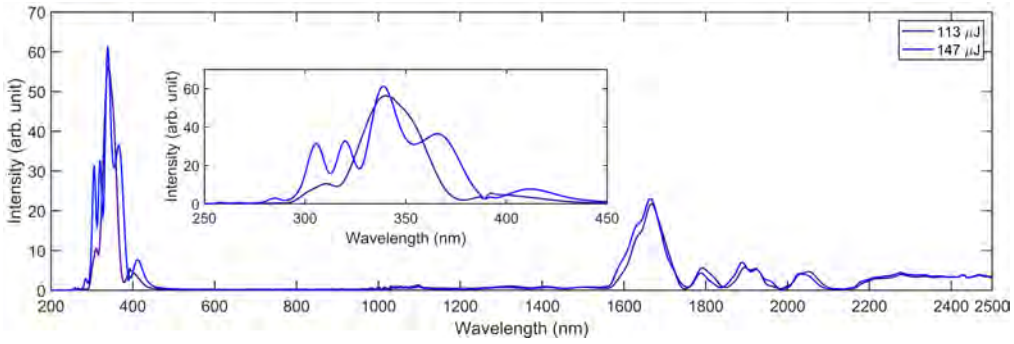

Figure 3.21: Spectra for broadening in Krypton at 113 µJ and 147 µJ. The inset zooms to the spectral region of the dispersive waves.

XPM and SPM could be the cause of this. But still, other effects arising from higher order mode coupling and plasma interaction can occur. In the following chapter, simulations are performed to verify if these supercontinua, including the modulated RDW at higher input pulse energy, can be reproduced.

Chapter 4

Numerical Simulations

In this chapter some results obtained by numerical simulations are discussed. The aim is to find out if the generation of a dispersive wave is possible, and if, how well the wavelength and intensity match the measurements. In addition, the general broadening behaviour is evaluated with respect to the point of fission and the subsequently diminishing VIS spectrum.

The used program is PyNLO, which is a free package for Python [30]. It simulates the propagation of a laser beam by computing the pulse both in time and frequency domain at every small travel distance inside the fibre. At each step the physical processes described in the GNLSE, shown in section 1.2, are applied to the pulse. The method used is the the adaptive-step-size fourth-order Runge-Kutta in the Interaction Picture [31]. The coefficients α and γ that are contained in this equation were calculated with the equations 1.25 and 1.26. Although these parameters are wavelength dependent, the simulation treats them as constants computed at the central wavelength of 2000 nm. The listed beta coefficients were not calculated. Instead, the program was modified to accept the dispersion curve that is the result of evaluating equation 1.29. The fibre length was set to 30 cm, the fibre core diameter to 200 µm and the temperature to 297 K to match the experimental conditions.

The program accepts a custom spectrum with spectral phase as an input for the simulation. Two different input spectra were created. They are shown in figure 4.1. The first is a fit of four Gaussian functions. For this, the sum of four single Gaussian bell curves was fitted to the measured spectrum that was shown in figure 3.1. With this approximation, the simulations ran fine with the pulse energy of 80 µJ. For higher pulse energies, as it was used in the energy scan, another input spectrum was needed in order to have a stable simulation. A Supergaussian of sixth order was working fine, as it is very smooth with comparable bandwidth to the original spectrum. Both spectra have in common that they do not include the residual OPCPA light around 1000 nm, as it does not take part in super continuum generation. The spectral phase was set to zero for both spectra, meaning that an ideal compressed pulse was used for the

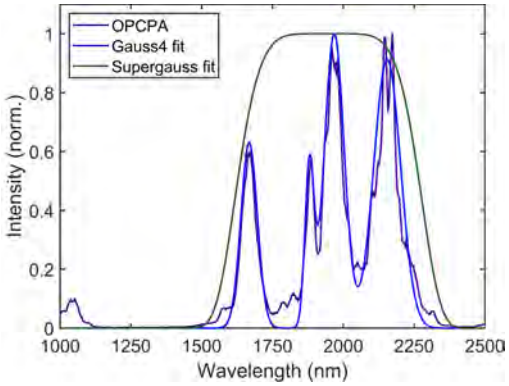

Figure 4.1: Fitted input spectra used for the simulations. The OPCPA spectrum is the same as in figure 3.1.

simulations. In order to achieve comparable simulation results between these two input spectra, the pulse energy was reduced for the Supergaussian fit in order to have the same temporal peak intensity as the Gauss4 fit. This was realized by multiplying the real pulse energy by a factor of 0.58 in the program. The first simulations were aimed at determining the wavelength of the dispersive wave, if it is generated. The results are shown in figure 4.2. Here, the measured

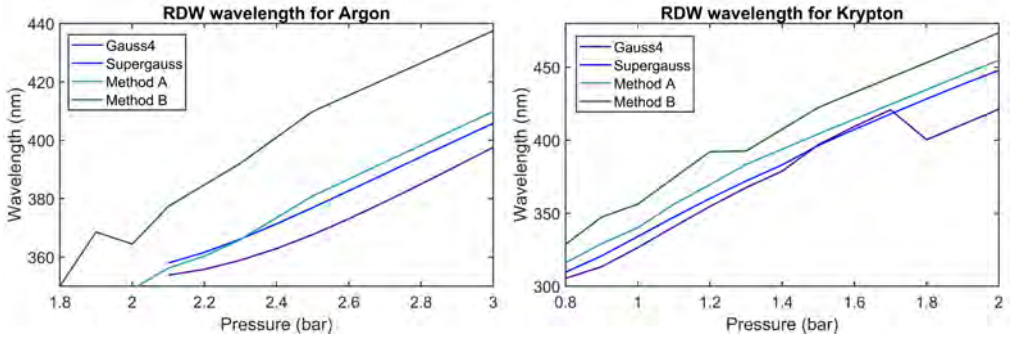

Figure 4.2: Simulated RDW wavelength compared to the measured values for both gases. The simulations were done with the two input spectra shown in figure 4.1.

wavelengths, which have already been shown in chapter 3, are compared to the results of the simulations. Both input spectra were used, where 80 µJ was set in the program for the Gauss4 fit and a reduced energy for the Supergauss fit as mentioned. One can clearly see that the simulated wavelengths are close to the values obtained with method A. Especially by considering that the distance to method A is smaller than the distance between both methods A and B, it shows that the simulations do a good job in prediction the wavelength of

the dispersive wave. Also the curvature agrees well with the measured curves, indicating that for another pressure range the simulations will also give satisfying results. Whereas for Krypton every simulated spectrum has a RDW, for Argon a dispersive wave only starts to appear above 2.1 bar. The reason could be that in the simulations there was no energy transfer yet or it was so minuscule that it did not lead to a pronounced dispersive wave. As it will be shown in the following, the simulated RDW is in general relatively weak.

Now, the output spectra are compared to the real spectra from the measurements. In the last chapter one could see, that the spectra from Krypton and Argon were comparable, as the pressure range was adapted so that the nonlinear effects are roughly the same. This is the same for the simulations, where the different gases produced comparable output spectra for their own pressure range. Following from this it is not necessary to shown the spectra for both Argon and Krypton in order to determine the accuracy of the program, especially as it was already proven that the simulated wavelengths of the dispersive waves match the measured values. So, the simulated and measured output spectra for Krypton at 1 bar, 1.5 bar and 2 bar are shown in figure 4.3. For the input spectrum, the fit Gausss4 was selected, as this spectrum has more in common with the OPCPA spectrum than the fit Supergauss. The first thing to notice is that the RDW is much weaker than the NIR part in the simulations than in the measurements. A possible explanation can be that the program takes the attenuation α as a constant. This is of course not true, as it can be seen from equation 1.25 that it is wavelength dependent and increases quadratically with it. This means that a dispersive wave around 400 nm should experience a attenuation constant 25 times lower than for the input pulse at 2 µm. But still, this would then require some propagation inside the fibre to show an effect. If the fission happens close to the fibre end, which was found out to the case for 1 bar, the different attenuation values should not show a strong influence on the relative spectral intensity of the dispersive wave. So, there must be also other effects explaining why the RDW is so strong in the measurements. No surprise are the missing interference fringes around 1000 nm, as this residual light was not included in the input spectra. The simulated NIR part shows clearly modulations due to SPM and self steepening, which agrees to some extend to the measured spectrum. Although the used NIR spectrometer has its limit at 2500 nm, the spectrum was extended to 3600 nm to see what the simulations show for this region.

Since the program solves the GNLSE for every travelled step inside the fibre, it computes the spectrum and the pulse in time for every propagated distance. The resulting spectral evolution inside the fibre of the three just shown output spectra is illustrated in figure 4.4.

Here, the behaviour of the supercontinuum generation from SPM and self steepening with subsequent dispersive wave generation can be identified for every pressure. At first, the input pulse, which is a soliton as it lies in the anomalous

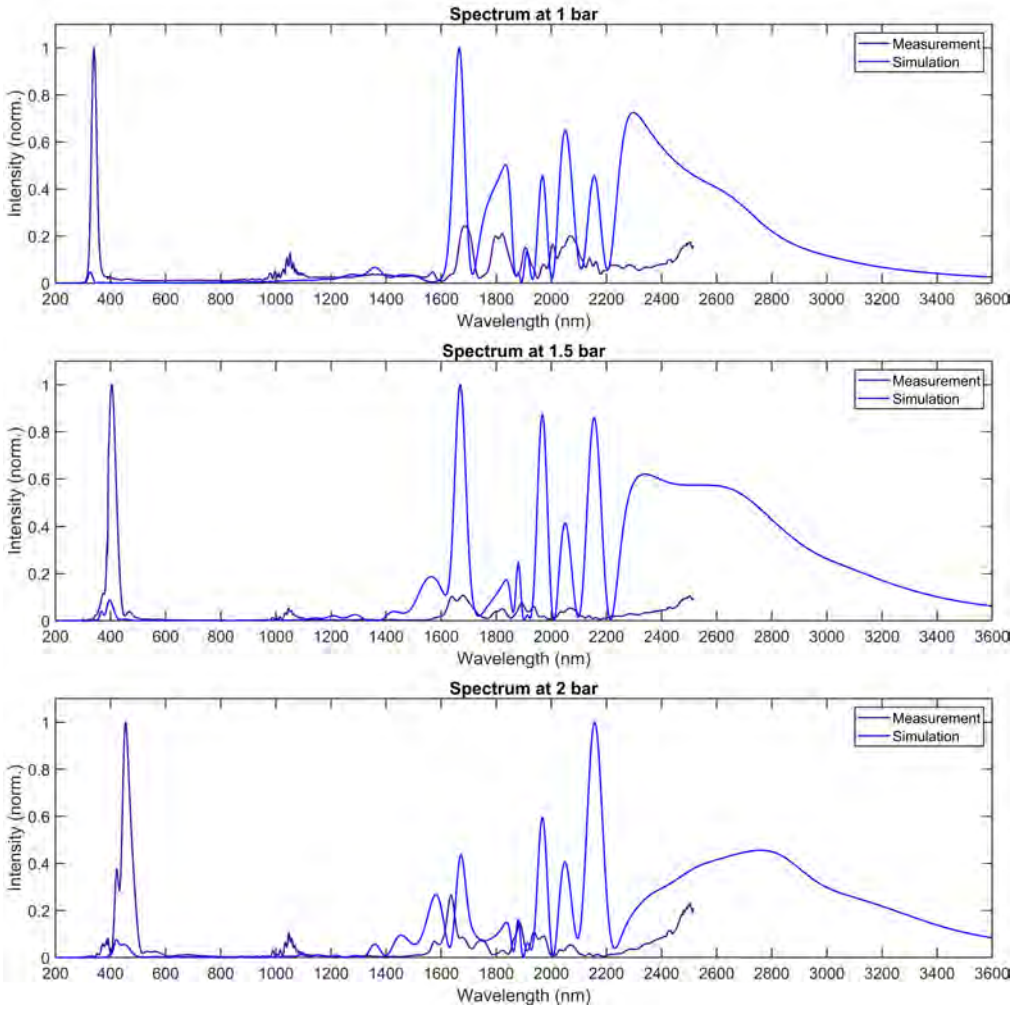

Figure 4.3: The simulated output spectra for Krypton at different pressures are compared to the measurements. Gauss4 fit is used as the input spectrum.

dispersion region of the fibre, broadens up to the UV followed by a resonant transfer of energy to the dispersive wave. When the fission length is reached, the soliton will break up, which results in the RDW to travel on its own and a slow disappear of the VIS light. The different behaviour at different pressures was already indicated during the discussion of the measured data. Here, it can be seen again that the fission length decreases with increasing pressure. This time, however, the results are more accurate than the characteristic length scales that were shown in chapter 3. From the evaluated measured spectra it could be deduced that the fission length equals the fibre length at about 1 bar, as for higher pressures the VIS light started to vanish and also the spectral

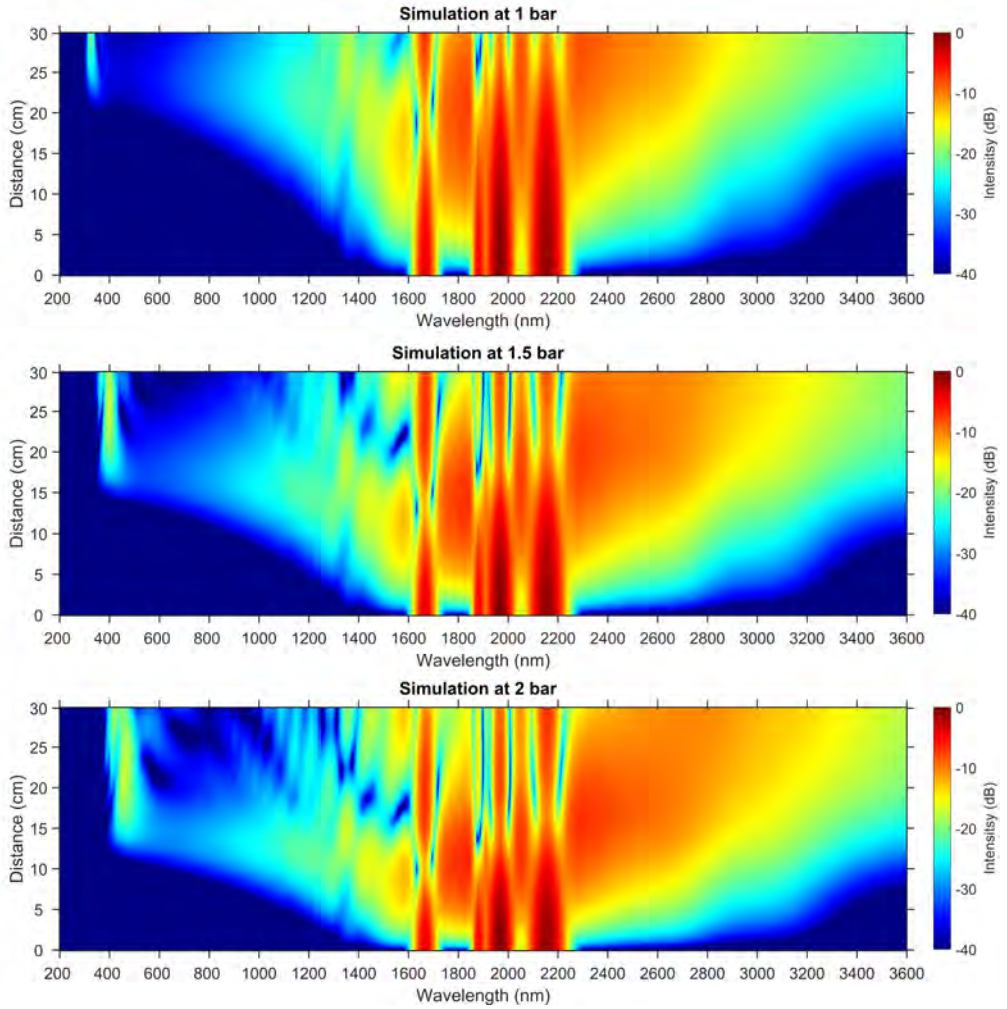

Figure 4.4: Simulated spectral evolution of broadening in Krypton at three different pressures. Gauss4 fit is used as the input spectrum.

intensity did not change much. The simulations agree with that, as for 1 bar fission already happened before the end of the fibre. This is because the broadened light between input pulse and RDW starts to fade away. With a further increase in pressure, the fission length becomes shorter and shorter, leading to a weaker overall broadening at the output. Furthermore is the value of the RDW wavelength increasing. What could not be seen in the measurements is that for higher pressures the broadening in the VIS region seems to be stronger before the fission happens, as the fibre was longer than that fission length.

Next, the simulated output pulse in the time domain is illustrated in figure 4.5. Here, the envelope of the pulse as it leaves the fibre is shown for the same

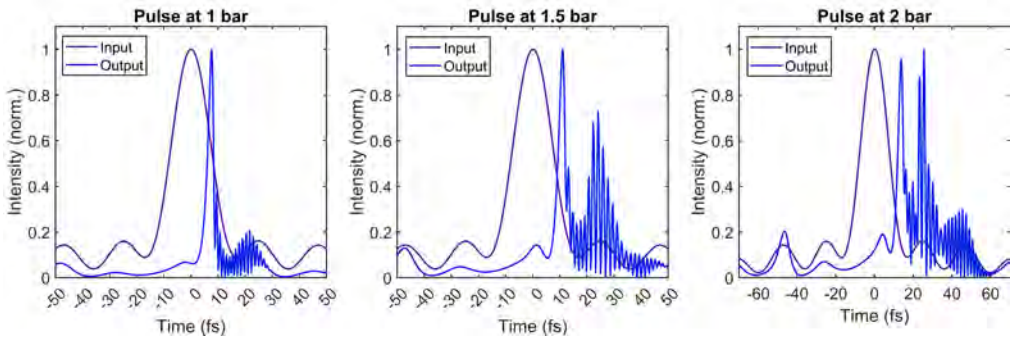

Figure 4.5: Simulated pulse envelope at the output for broadening in Krypton at three different pressures. Gauss4 fit is used as the input spectrum.

three different pressures. It is clearly visible that the output pulse is shorter than at the input, which is caused by the anomalous dispersion of the fibre. Additionally the effect of self steepening can be identified by the trailing edge. It also shows fast modulations, that fall further behind as the pressure increases. These modulations are coming from the high frequency components that were necessary for the very steep trailing edge. But as the pulse broke up, they started to lag behind since the refractive index is higher for them than for the rest of the pulse. And with increasing pressure, the temporal distance between the NIR pulse and the short wavelengths increases because they are generated earlier inside the fibre.

Now, the RDW should be investigated at higher input pulse energies. For this, the computed output spectra for just the dispersive waves alongside the RDW obtained from the measurements are shown in figure 4.6. In chapter 3 it was shown that the dispersive wave gets broader and spectrally modulated as the input pulse energy was increased. For the simulations, the input spectrum Supergauss fit was used. The other spectrum, Gauss4 fit, caused problems during the simulations and did not give valuable results. It can be seen that the spectrum shows some modulations at the highest pulse energy, but still not comparable to the strength of the measured one. In addition is the spectral bandwidth not as large. In chapter 3 is was suggested that XPM or SPM can be the cause. If this is really the case, the simulations do not show this for two possible reasons. Firstly, the intensity of the RDW compared to the NIR is weak, so it might not be sufficient high for SPM on its own. Secondly, the nonlinear coefficient γ is treated as a constant in the simulations. This is not true since it does increase with shorter wavelengths. As a result, the simulated nonlinear strength is weaker than it is in reality. But, if it is caused by the output window, it can of course not be explained by the simulations. Additionally, the mentioned contribution from higher order modes cannot be simulated as well as plasma effects, as they are not included in the numerically solved GNLSE.

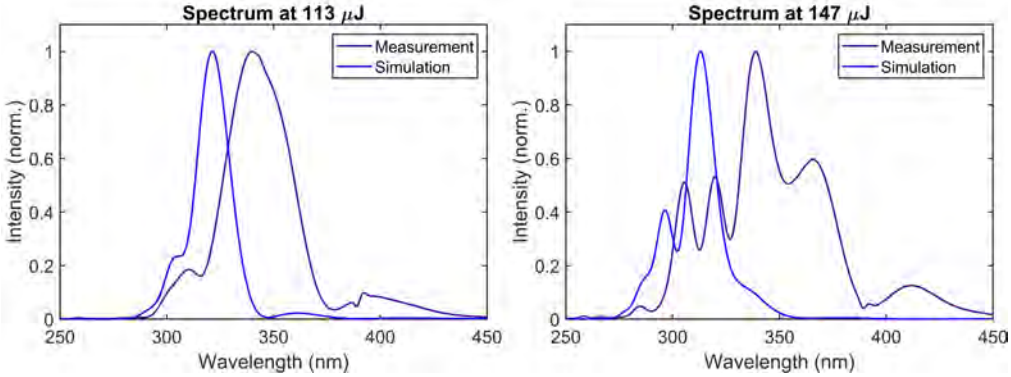

Figure 4.6: Simulated RDW spectrum for input pulse energies of 113 µJ and 147 µJ for broadening in Krypton alongside the measurement. Supergauss fit is used as the input spectrum.

An additional simulation was performed to see if SPM can generate such a spectrum. Here, the simple assumption was made that the dispersive wave is just a pulse with a specific energy and spectral bandwidth that is propagating inside a fibre. The result is shown in figure 4.7. In this case, just a UV pulse

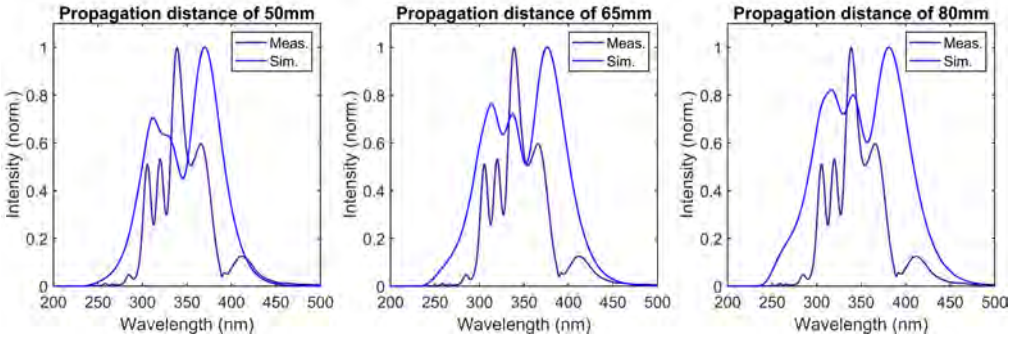

Figure 4.7: Simulated spectrum if just a UV pulse is propagating inside a Krypton filled fibre at 1 bar. The initial UV spectrum is comparable with the dispersive wave illustrated in figure 3.19. The conversion efficiency is assumed to be 20 %. The resulting spectrum after a specific propagation distance is compared to the measured spectrum of the RDW with the input pulse energy of 147 µJ.

was used as the input for a Krypton filled fibre at 1 bar. The spectrum was a Gaussian centred at 340 nm with a spectral width of 20 nm. This is comparable to the spectrum of the RDW shown in figure 3.19. The pulse energy was set to $0.2 \cdot 147\,\mu\text{J} = 29.4\,\mu\text{J}$. The conversion efficiency of 20 % was determined by numerically integrating the measured spectra to get an esimation of how much

energy is contained in the RDW and applying the total transmission efficiency of 45 %. This time, the nonlinear coefficient and the attenuation constant are calculated at the center wavelength of the UV pulse and not the NIR soliton. Simulations have shown that the fission happens somewhere a the middle of the fibre, which results in a propagation length for the RDW to be 15 cm at maximum. The simulated spectra show clearly broadening of the pulse, now reaching more than 100 nm with respect to the 20 nm at the beginning. This time, the bandwidth of the simulated pulse is also closer to the measured spectrum in contrast to what was illustrated in figure 4.6. Modulations are also present, even though not in the extent of the measured spectrum. Below 50 mm there is a dip in the centre of the spectrum. After some more propagation a third peak starts to appear, which is visible at 65 mm. For an even longer travel distance the peaks starts to become more equal in hight, which is indicated at a distance of 80 mm. Therefore, SPM can indeed broaden the RDW and cause spectral modulations given the contained pulse energy and perfect compression. But still, the simulated spectra do not equal the measured ones. This means that a further interaction with the main NIR pulse causes the shape of the RDW. This includes the already mentioned coupling to higher order modes or the generation of several dispersive waves that interfere with each other.

Chapter 5

Conclusion and Outlook

In chapter 3, where the experimental measurements were analysed, it was shown that there are three states of broadening. The first is described by a spectral range that reaches the UV, but without the presence of a dispersive wave. The second state is described by the build up of a dispersive wave with an additional increase of general broadening, so in the NIR and VIS region. The propagating pulse is still the higher order soliton in this state. It did not yet undergo fission, although experiencing self compression due to the anomalous dispersion. The third and last state is reached after soliton fission. There, the original soliton breaks up and the residual ones can not support the broad spectrum anymore, which results in less general broadening as the VIS disappears. The RDW is strongest in this state, as there was a continuous energy transfer until the fission.

During the pressure scan it was observed that both gases can produce a supercontinuum. The main difference is that for a comparable spectrum the pressure is lower for Krypton. However, for a state where a transfer of energy to the dispersive wave has happened but did not yet lead to a pronounced peak, Krypton seems to generate a more broadband spectrum. This is the case as due to the phasmatching condition the RDW is positioned at shorter wavelengths for Krypton. For both gases, the further increase in pressure led to a very strong RDW and a longer wavelength of which. An additional energy scan showed another behaviour. The wavelength did not change much and the maximum spectral intensity did not increase with higher input pulse energy. Instead, the RDW started to show a strong spectral modulation and broadening.

In chapter 4, the simulated spectra were compared to the measurements. It was shown that the wavelength of the dispersive wave agrees well with the measured value when the pressure was changed. Also the fission length seems to agree with the experiment. Only the relative spectral intensity compared to the NIR part is too low with respect to the measurements. The measured spectral broadening of the RDW at higher pulse energies could also not really be achieved. But as a tool to figure out the wavelength of the generated RDW, as well as to determine the fission length, it seems to work well.

With this in mind, the first conclusive outlook can be made. The aim of this thesis was to analyse the generated spectrum, especially the origin of the dispersive wave. One goal was to estimate the supercontinuum the next generation synthesizer will have. The source to achieve this is a 2 µm beam with a pulse energy of 80 µJ. From the measurement series it could already be seen that a super continuum without a pronounced dispersive wave can be generated using a 30 cm long fibre at 0.7 bar for Krypton or 1.8 bar for Argon. A requirement for this is that the fission would happen after the fibre ends, since only a very limited transfer of energy is wanted. As a result, the broadband spectrum is flat due to the missing RDW. To suppress the generation of a dispersive wave, the fibre has to end shortly after the spectrum has broadened into the UV due to SPM and self steepening. This has a positive effect on pulse compression. Every wavelength below the zero dispersion wavelength experiences normal dispersion, which especially affects the shorter wavelengths of the spectrum. If the fibre ends shortly after the generation of those, the total dispersion they accumulate is limited. This is in contrast to the case where a RDW is generated, as here the short wavelengths propagate a longer distance inside the fibre and thus getting more dispersed. The shorter propagation inside the fibre has the advantage that the amount of chirped mirrors for post compression inside the synthesizer is reduced. To further improve the intensity of the broadband spectrum, the pressure can be increased by simultaneously decreasing the fibre length. The simulations have shown that the spectral region between the dispersive wave and the input pulse, at a propagation distance where the RDW is still weak, gets stronger with higher pressures. To suppress the generation of the dispersive wave, the fibre has to be shortened accordingly to that specific propagation distance. This would also results in an improved transmission of the power, as the total attenuation of the beam decreases as the fibre length does. But still, it should be noted that the spectral intensity might increase with higher pressures, the total bandwidth however might decrease as the wavelength of the RDW gets longer. Further simulations can help to determine the optimal pressure to guarantee a broadband and intense supercontinuum.

The second conclusive outlook is about the generated RDW. This can be an intense laser source for UV light. Although the simulations could not show it, in the measured spectra it is clearly visible that the generated dispersive waves are intense. A further measurement series could focus on determining the conversion efficiency to see how much energy is confined in this UV region. But since it could already be seen that the peak has quite some spectral intensity, the possibility to change the wavelength of that dispersive wave makes it an intense and tunable UV source. And if the conversion efficiency is even high enough to support the assumption that the RDW has enough energy that broadening due to SPM is affecting it, another measurement series could focus on broadband UV generation.

Appendix A

Data Archiving

The experimental raw data, the matlab evaluation files, the presented figures, the python program and the modified Python package PyNLO are archived on the server of the Laboratory for Attosecond Physics at the Max Planck Institute of Quantum Optics:

//afs/ipp-garching.mpg.de/mpq/lap/publication_archive

The ReadMe file contains a detailed description of the organization of the raw data and how to use the evaluation files and the Python program.

Bibliography

[1] Jean-Claude Diels and Wolfgang Rudolph. *Ultrashort Laser Pulse Phenomena*. Second Edition. Burlington: Academic Press, 2006.

[2] Govind P. Agrawal. *Nonlinear Fiber Optics*. Fifth Edition. Kidlington: Academic Press, 2013.

[3] Robert W. Boyd. *Nonlinear Optics*. Third Edition. Burlington: Academic Press, 2008.

[4] Bahaa E. A. Saleh und Malvin Teich. *Optik und Photonik*. Dritte Auflage. Weinheim: Wiley-VCH, 2020.

[5] Ka Fai Mak. "Nonlinear optical effects in gas-filled hollow-core photonic-crystal fibers". PhD Thesis. Friedrich-Alexander Universität Erlangen-Nürnberg, 2014.

[6] John C. Travers et al. "Ultrafast nonlinear optics in gas-filled hollow-core photonic crystal fibers". In: *J. Opt. Soc. Am. B* 28.12 (Dec. 2011), A11–A26.

[7] John C. Travers et al. "High-energy pulse self-compression and ultraviolet generation through soliton dynamics in hollow capillary fibres". In: *nature photonics* 13 (Aug. 2019), 547–554, S1–S14.

[8] Christos Markos et al. "Hybrid photonic-crystal fiber". In: *Reviews of Modern Physics* 89.4 (Dec. 2017), 045003(55).

[9] C. Vozzi et al. "Optimal spectral broadening in hollow-fiber compressor systems". In: *Applied Physics B* 80 (2005), pp. 285–289.

[10] Carsten Brée, Ayhan Demircan, and Günter Steinmeyer. "Method for Computing the Nonlinear Refractive Index via Keldysh Theory". In: *IEEE Journal of Quantum Electronics* 46.4 (Apr. 2010), pp. 433–437.

[11] B. H. Bransden and C. J. Joachain. *Physics of Atoms and Molecules*. Second Edition. Harlow: Prentice Hall, 2003.

[12] A. Börzsönyi et al. "Dispersion measurement of inert gases and gas mixtures at 800 nm". In: *Applied Optics* 47.27 (Sept. 2008), pp. 4856–4863.

[13] Thomas Roger et al. “High-energy, shock-front-assisted resonant radiation in the normal dispersion regime”. In: *Physical Review A* 88.9 (May 2013), 051801(5).

[14] Enrico Ridente et al. “Hybrid phase-matching for optical parametric amplification of few-cycle infrared pulses”. In: *Optica* 7.9 (Sept. 2020), pp. 1093–1096.

[15] Thomas Metzger et al. “High-repetition-rate picosecond pump laser based on a Yb:YAG disk amplifier for optical parametric amplification”. In: *Optics Letters* 34.14 (July 2009), pp. 2123–2125.

[16] Mikhail Mamaikin. “Time-Resolved Microscopy of Near-Infrared to Visible Waveforms”. Ludwig-Maximilians-Universität München, 2020.

[17] Olga Razskazovskaya. “Infrared waveform synthesis for applications in attosecond science”. Ludwig-Maximilians-Universität München, 2017.

[18] Erik Robert Hosler. “Ultrafast Strong-Field Vibrational Dynamics Studied by Femtosecond Extreme-Ultraviolet Transient Absorption Spectroscopy”. University of California, Berkley, 2013.

[19] F. A. Ilkov, J. E. Decker, and S. L. Chin. “Ionization of atoms in the tunnelling regime with experimental evidence using Hg atoms”. In: *Physical Review Letters* 25.19 (1992), pp. 4005–4020.

[20] F. Tani, J. C. Travers, and P. St. J. Russel. “PHz-wide Supercontinua of Nondispersing Subcycle Pulses Generated by Extreme Modulational Instability”. In: *Physical Review Letters* 111 (3 2013), 033902(5).

[21] Ka Fai Mak et al. “Tunable vacuum-UV to visible ultrafast pulse source based on gas-filled Kagome-PCF”. In: *Optics Express* 21.9 (2013), pp. 10942–10953.

[22] Guoqing Chang, Li-Jin Chen, and Franz X. Kärtner. “Fiber-optic Cherenkov radiation in the few-cycle regime”. In: *Optics Express* 19.7 (Mar. 2011), pp. 6635–6647.

[23] Guoqing Chang, Li-Jin Chen, and Franz X. Kärtner. “Highly efficient Cherenkov radiation in photonic crystal fibers for broadband visible wavelength generation”. In: *Optics Letters* 35.14 (2010), pp. 2361–2363.

[24] F. Köttig et al. “Mid-infrared dispersive wave generation in gasfilled photonic crystal fibre by transient ionizationdriven changes in dispersion”. In: *Nautre Communications* 8 (1 Sept. 2017), pp. 1–8.

[25] D. Novoa et al. “Photoionization-Induced Emission of Tunable Few-Cycle Midinfrared Dispersive Waves in Gas-Filled Hollow-Core Photonic Crystal Fibers”. In: *Physical Review Letters* 115 (July 2015), 033901(5).

[26] A. Ermolov et al. “Supercontinuum generation in the vacuum ultraviolet through dispersive-wave and soliton-plasma interaction in a noble-gas-filled hollow-core photonic crystal fiber”. In: *Physical Review A* 92.3 (2015), 033821(7).

[27] Francesco Tani, John C. Travers, and Philip St. J. Russel. “Multimode ultrafast nonlinear optics in optical waveguides: numerical modeling and experiments in kagomé photonic-crystal fiber”. In: *J. Opt. Soc. Am. B* 31 (2 2014), pp. 311–320.

[28] W. Chang et al. “Influence of ionization on ultrafast gas-based nonlinear fiber optics”. In: *Optics Express* 19.21 (2011), pp. 21018–21027.

[29] P. Hölzer et al. “Femtosecond Nonlinear Fiber Optics in the Ionization Regime”. In: *Physical Review Letters* 107 (20 2011), 203901(5).

[30] *PYNLO*. 2021. URL: `https://github.com/pyNLO/PyNLO`.

[31] Johan Hult. “A Fourth-Order Runge–Kutta in the Interaction Picture Method for Simulating Supercontinuum Generation in Optical Fibers”. In: *Journal of Lightwave Technology* 25.12 (Dec. 2007), pp. 3770–3775.

Acknowledgements

First, I would like to thank Ferenc Krausz for giving me the opportunity to join his group and making it possible to work with an advanced laser system.

Secondly, I would like to thank Matthew Weidman for showing me the possibility to enter the world of ultra fast physics by writing this thesis.

Furthermore am I especially thankful to Mikhail Mamaikin and Najd Altwaijry for always being helpful and teaching me how to work in the lab and maintain it, included countless hours of fixing the laser system.

Also, I would like to thank Eva Bayer. Although you could not see what this mysterious peak in the UV is in the time you where here, at some point you get to know and you will be enlightened.

Next, I would like to thank Amelie Schulte and Corinna Konrad for being nice office colleagues, at least for the limited time I was not in the lab.

Last, I would like to thank Muhammad Qasim for being a good lab colleague, who did in particular not touch, although needed, my third power supply for the spectrometer after the first two disappeared without a trace.

Eidesstattliche Erklärung

Hiermit erkläre ich, die vorliegende Arbeit selbständig verfasst zu haben und keine anderen als die in der Arbeit angegebenen Quellen und Hilfsmittel benutzt zu haben.

München, 13.09.2021 Michael Heynck